EES Solar

ROYAL SOCIETY OF CHEMISTRY

ANALYSIS

View Article Online
View Journal | View Issue

Cite this: *EES Sol.*, 2026, **2**, 273

Electrochemical direct air capture with intermittent renewable energy: techno-economic insights from solar-driven electrodialysis systems

Guokun Liu,[a] Yukun Zhang,[a] Meng Lin *[b] and Aidong Yang*[a]

Electrochemical direct air capture (DAC) driven by renewable electricity offers a fully electrified pathway for scalable carbon removal, yet its integration with intermittent renewable power and the resulting system-level constraints remain poorly understood. Here we present a comprehensive techno-economic assessment of bipolar membrane electrodialysis (BPMED)-based DAC systems powered by solar electricity, explicitly accounting for diurnal and seasonal variability, energy storage requirements, and operational flexibility. Using a physics-based, time-resolved modelling framework with real solar irradiance data, we evaluate three representative configurations: battery storage, integrated hydrogen production, and decoupled hydrogen generation. While battery storage achieves the lowest specific energy consumption (430 kJ per mol-CO_2), hydrogen-based configurations are more cost-effective for long-duration storage under strict off-grid operation. Flexible BPMED load reduces seasonal storage demand, yielding a minimum DAC cost of 2163 $ per t-CO_2. We further show that electricity supply flexibility, enabled by limited grid assistance, defines a practical lower bound on system-level electricity costs, enabling LCOEs below 100 $ MWh^{-1} and DAC costs below 1000 $ per t-CO_2. Under favorable future scenarios (50 $ MWh^{-1} electricity and 100 $ m^{-2} membrane cost), BPMED-based DAC costs are projected to decrease to 330 $ per t-CO_2. Beyond BPMED-specific results, this work identifies generalizable constraints and design principles applicable to electrochemical DAC technologies under renewable electricity supply.

Received 6th February 2026
Accepted 9th February 2026

DOI: 10.1039/d6el00018e

rsc.li/EESSolar

Broader context

Electrochemical direct air capture (DAC) offers a modular pathway for CO_2 removal that can, in principle, pair directly with renewable electricity. Its practical competitiveness, however, is set not only by cell-level efficiency and durability, but also by the cost of delivering electricity under intermittency and the need for short- and long-duration energy storage. Bipolar membrane electrodialysis (BPMED) is a representative electrochemical regeneration approach that avoids thermal input and redox mediators, making it a useful platform to quantify these coupled constraints. Here we perform a time-resolved, system-level techno-economic analysis of BPMED-DAC under intermittent solar supply, compare multiple storage and operating configurations (including hybrid/grid-assisted baselines), and benchmark against commercial DAC technologies. The study translates device metrics into system-level design rules and performance targets, clarifying when electrochemical DAC can be competitive and what improvements are required under realistic renewable constraints.

Introduction

The rising concentration of carbon dioxide (CO_2) in the atmosphere is a primary driver of global climate change, with far-reaching environmental and socio-economic implications.[1,2] Current projections indicate that, without immediate and decisive intervention, the remaining carbon budget to limit global temperature increase to 1.5 °C could be depleted by 2030.[3] While the reduction of greenhouse gas emissions remains paramount, negative emission technologies, such as direct air capture (DAC), have become essential complements to decarbonization strategies in achieving net-zero emission targets.[4]

In contrast to temperature-swing DAC systems such as those developed by Carbon Engineering, which rely on high-temperature calcination (~900 °C) and are typically powered by natural gas combustion, electrochemical pH-swing DAC offers a fundamentally different pathway, one that is fully electric, modular, and potentially easier to integrate with renewable energy sources. This electrified approach eliminates fossil-fuel dependency for regeneration and reduces the carbon intensity and siting constraints of DAC infrastructure. Among electrochemical methods, bipolar membrane electrodialysis (BPMED) uniquely enables a continuous, thermally

[a]*Department of Engineering Science, University of Oxford, Oxford OX1 3PJ, UK. E-mail: aidong.yang@eng.ox.ac.uk*

[b]*Department of Mechanical and Energy, Southern University of Science and Technology, Shenzhen 518055, China. E-mail: linm@sustech.edu.cn*

independent pH-swing without external chemical inputs, using only water dissociation within the membrane stack. This pH-swing mechanism relies on manipulating the solubility and speciation of inorganic carbon (CO_2, bicarbonate, and carbonate) *via* electrolytic basification-acidification cycles of aqueous media, thereby enabling reversible CO_2 absorption and release.[5,6] These features position BPMED as a promising platform for sustainable DAC, particularly when coupled with intermittent renewable electricity such as solar PV. However, BPMED integration with variable energy supply remains underexplored, and tradeoffs among storage strategies lack rigorous quantification.

Currently, the most developed and widely deployed DAC technologies can be broadly categorized into adsorption (amine-scrubbing) and absorption (wet-scrubbing), depending on the sorbent employed.[7,8] The solid adsorption method has received more attention in the research and development of DAC,[9,10] as it offers higher volumetric productivity and a lower regeneration temperature of 80–130 °C.[8] Companies such as Climeworks[11,12] and Global Thermostat[13] have adopted this approach, and a commercial plant in Iceland has demonstrated its feasibility at a current cost of 500–600 $ per t-CO_2.[14,15] However, several challenges remain, including uncertainties in adsorption mechanisms,[8,16] heat transfer limitations,[17] and material degradation.[18,19] Additionally, solid adsorbents require batch processing, necessitating periodic cycling of sealing and operating conditions (temperature, pressure, or humidity).[20] The complexity of adsorbent design and batch operation leads to high construction costs of air contactor (adsorber) and relevant components, posing a fundamental barrier to further cost reductions. As a result, current adsorption-based DAC technologies remain far above the widely cited target of approximately 100 $ per t CO_2 required for large-scale economic feasibility. By contrast, liquid absorption using an alkali solution is considered a technically simpler and more mature capture method. The DAC plant developed by Carbon Engineering[21,22] has demonstrated continuous atmospheric CO_2 absorption using an alkali solution loop. Their air contactor design, adapted from cooling towers,[22,23] allows the continuous flow of aqueous absorbent through PVC packing, effectively capturing CO_2 from air. This wet-scrubbing air contactor enables continuous operation and adjustable load control, while also offering greater longevity and lower costs for both the absorbent and the facility. According to Keith *et al.*,[22] the capital cost of a wet-scrubbing air contactor is 136 $/(t-$CO_2$ per year), whereas an amine-scrubbing adsorber costs 900 $/(t-$CO_2$ per year).[24] The total cost of Carbon Engineering's process is projected to decrease to 94–232 $ per t-CO_2,[15,22] which is considered economically competitive with adsorption-based DAC methods. The pH-swing process, which is based on aqueous solutions, can be integrated with the wet-scrubbing process to establish a continuous DAC cycle. Its combination with the wet-scrubbing process offers the potential for flexible operation and cost-effective CO_2 capture compared to common solid-adsorbent systems.

In addition to the wet-scrubbing capture method, another advantage of the electrochemical pH-swing lies in its regeneration method. The high thermal energy demand for sorbent regeneration has been widely recognized as a major challenge in temperature-swing DAC technologies.[25] In general, existing temperature-swing DAC systems require total energy inputs (thermal energy and electricity) of approximately 300–400 kJ per mol-CO_2,[26] which constitutes a substantial portion of the overall operational cost.[8] Particularly, in Carbon Engineering's wet-scrubbing process, a large amount of high-temperature (approximately 900 °C (ref. 22)) thermal energy is required for calcining solid carbonate to release CO_2 and regenerate the alkali solution. This high-grade heat is typically sourced from natural gas combustion, leading to additional CO_2 emissions, high costs, and fuel dependency. By contrast, the electrochemical pH-swing process enables sorbent regeneration under ambient temperature conditions, with energy requirements met entirely by renewable electricity, thereby eliminating the need for thermal energy of any grade. Additionally, advancements in electrochemical system design and precise control of operating conditions are expected to further reduce energy consumption, reinforcing the electrochemical pH-swing process as a more energy-efficient alternative to temperature-swing methods, with demonstrated energy requirements below 100 kJ per mol-CO_2.[27,28]

Several electrochemical systems for inducing a pH-swing have been proposed and investigated for their potential to achieve low energy consumption in CO_2 capture, including electrolysis,[29,30] capacitive deionization,[31,32] and proton-coupled electron transfer.[33,34] Among these, bipolar membrane electrodialysis (BPMED) stands out as particularly promising for scalable DAC applications. Bipolar membranes (BPMs) facilitate the dissociation of water into protons (H^+) and hydroxide ions (OH^-) without requiring additional chemical reactions. This capability allows BPMED to achieve a wide-range pH-swing with minimal electric potential and low energy consumption.[35] Furthermore, BPMED systems feature a relatively simple electrochemical configuration, avoiding the technical complexities and uncertainties associated with elaborate cell designs, intermediate reactions, or specialized electrolytes. Eisaman *et al.*[36–38] conducted a series of investigations on BPMED for CO_2 separation from carbonate/bicarbonate solutions, reporting an energy consumption of only 100 kJ per mol-CO_2 for regenerating gaseous CO_2. Incorporating the energy required for CO_2 capture from air into hydroxide solutions, they suggested that total DAC energy consumption could be as low as 300 kJ per mol-CO_2, which is competitive against existing plants. Building on the foundational work by Eisaman *et al.*,[36–38] subsequent studies have advanced the innovation and optimization of BPMED systems for CO_2 capture at the laboratory scale,[39–42] consistently reporting similarly low energy requirements. Sabatino *et al.*[43,44] conducted the first comprehensive evaluation of a scaled-up DAC process using BPMED, assessing its integration into a liquid solution loop analogous to Carbon Engineering's chemical looping process. Their findings offer valuable insights for assessing the feasibility of BPMED for large-scale DAC deployment. Beyond DAC, BPMED systems have also been adapted for CO_2 capture from other dilute sources, such as seawater,[45–48] further demonstrating their versatility and flexibility. Collectively, these studies have proved the feasibility of BPMED and its promise as a low-energy pathway for carbon removal applications.

The promising potential of BPMED and other electrochemical DAC systems is fundamentally predicated on the availability of renewable electricity as the primary energy input, offering a more sustainable and environmentally benign pathway for carbon removal.[35,49] However, a major challenge lies in coupling these systems with intermittent renewable sources such as solar and wind, which can undermine operational stability and accelerate material degradation.[50] Overcoming these fluctuations requires advanced energy storage solutions or flexible operation to align DAC performance with renewable energy availability.[51] Moreover, rigorous evaluation of DAC systems under real-world conditions is essential, especially under variable renewable energy inputs. Unlike ideal and levelized energy-supply scenarios in most existing literature,[22,43,44,52] practical conditions call for robust modeling of factors such as seasonal energy variability, geographical differences in energy costs, and the scalability of energy storage systems. Addressing these challenges is essential for advancing the large-scale implementation of electrochemical DAC technologies such as BPMED.

In this study, we investigate the integration of BPMED with intermittent renewable electricity to enable continuous pH-swing-driven DAC. To address the challenges imposed by renewable (solar) energy variability and seasonal intermittency, we evaluate three representative energy-storage configurations using a time-resolved, system-level modeling framework that couples electrochemical cells, sorbent regeneration, electricity generation, and energy storage. The analysis progresses from representative diurnal simulations to year-long simulations incorporating real-world meteorological and solar irradiance data, enabling quantitative assessment of practical techno-economic performance. We further examine how operational flexibility in BPMED current density and electricity supply flexibility, including grid-assisted operation, mitigate long-duration energy-storage requirements and reduce system cost. Beyond BPMED-specific results, this work identifies generalizable system-level constraints and design principles governing electrochemical DAC under renewable electricity supply, providing quantitative guidance for the design and deployment of next-generation electrochemical DAC technologies.

Results and discussion

Solar-driven DAC processes and system integration

Electrochemical DAC systems can be fully powered by electricity, offering a viable alternative to conventional thermally driven technologies. In this study, we evaluate the practical feasibility and operational performance of BPMED-based DAC

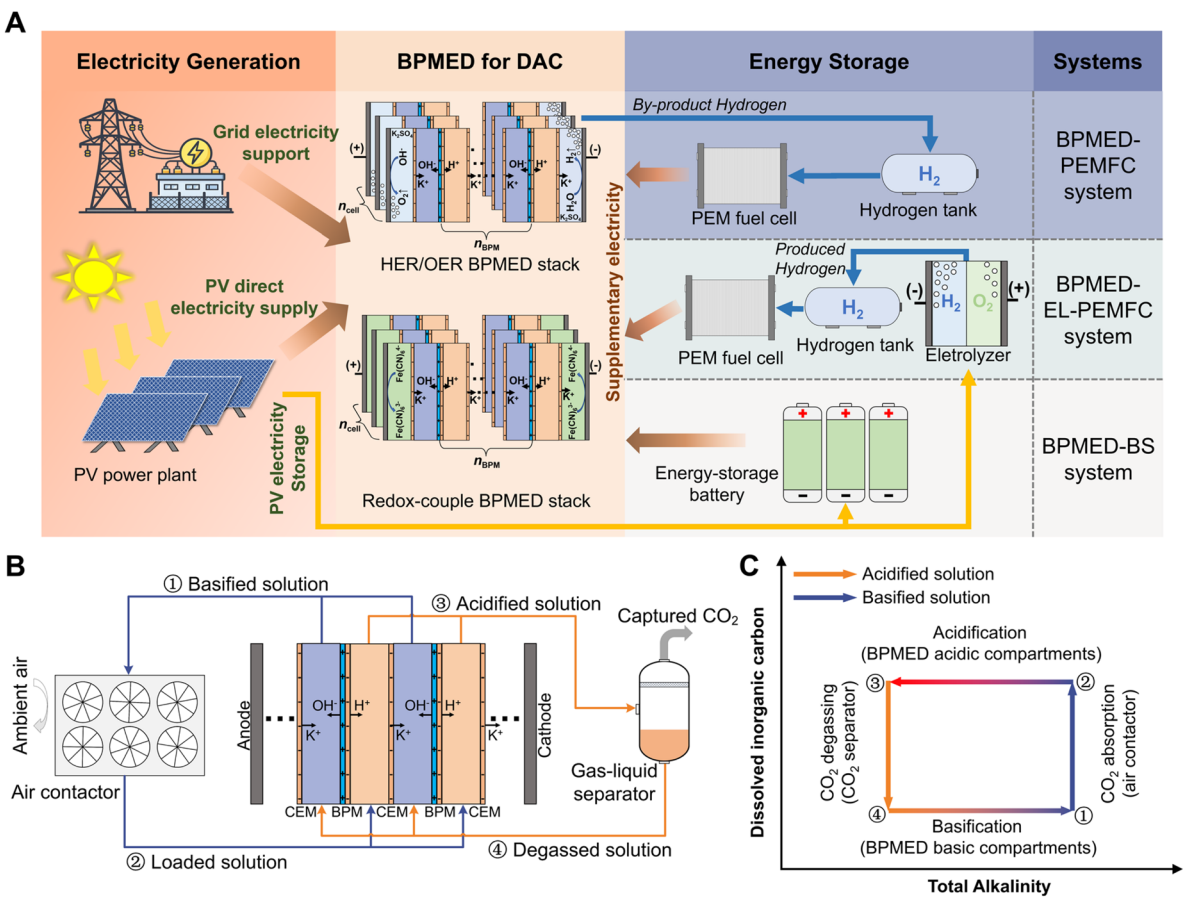

Fig. 1 Schematics of continuous solar-driven BPMED systems for DAC. (A) Components and energy flows of the integrated systems. (B) Solution regeneration process for continuous DAC operation. (C) Dissolved inorganic carbon-total alkalinity (DIC-TA) diagram illustrating solution regeneration.

systems under conditions where solar electricity serves as the primary energy input, while allowing for optional grid-assisted operation to ensure continuous and realistic system performance.

Fig. 1 illustrates the integrated system configurations and solution regeneration processes for DAC that are proposed, modeled, and assessed in this study. Electricity is primarily supplied by an on-site PV power plant, which directly powers the BPMED stacks during periods of sufficient solar generation. The inherent intermittency of PV electricity is managed through a combination of energy storage and electricity supply flexibility. Among available storage options, batteries and hydrogen-based storage are adopted and comparatively assessed due to their technological maturity and practical relevance.

Three potential system configurations are considered: BPMED-proton exchange membrane fuel cell (BPMED-PEMFC), BPMED-electrolyzer-proton exchange membrane fuel cell (BPMED-EL-PEMFC), and BPMED-battery storage (BPMED-BS), as illustrated in Fig. 1A. In all configurations, PV electricity is preferentially utilized to power BPMED operation. In addition to fully off-grid operation, the system framework allows grid-assisted electricity supply as a supporting operating mode. As shown in Fig. 1A, grid electricity is introduced only when instantaneous PV generation is insufficient to meet the electrical demand required for BPMED operation. Under such conditions, a fraction of the BPMED power demand can be supplied by the electricity grid, while PV electricity remains the dominant energy source whenever available. This grid-assisted configuration reflects realistic deployment and transitional operation scenarios, rather than assuming the grid as a continuous primary power source.

Each BPMED stack consists of n_{cell} single cells, with n_{BPM} repetitive BPM units (repetitive BPM-CEM structure) integrated into each cell. The electrochemical reactions occurring in the end compartments of the BPMED cells differ across system configurations.

BPMED-PEMFC system. Energy production for storage is integrated within the BPMED cell, where the hydrogen and oxygen evolution reactions (HER and OER) occur in the end compartments. The HER and OER establish an electric potential field that drives water dissociation in the BPMs, while simultaneously converting a portion of renewable electricity into hydrogen for energy storage. Hydrogen is generated as a by-product, stored, and later converted back into electricity *via* a PEMFC, providing supplementary power during periods of low PV supply. This integrated design mitigates repetitive over-potential losses compared to operating BPMED and HER electrolyzers as separate units, potentially enhancing both energy efficiency and system compactness. Although other electrochemical devices coupling energy storage with CO_2 capture have been developed previously,[53,54] these systems were not specifically designed for DAC and remain constrained to laboratory-scale feasibility. In this assessment, K_2SO_4 is employed as an inert supporting electrolyte in the BPMED end compartments.

BPMED-EL-PEMFC system. Hydrogen generation for the purpose of energy storage is decoupled from BPMED operation and performed in a separate electrolyzer. This configuration allows for flexible allocation of PV electricity between the BPMED and the electrolyzer for hydrogen storage. In contrast, in the BPMED-PEMFC system, HER and BPMED operations are interconnected (*i.e.*, they share the same operating current density). The $K_3/K_4Fe(CN)_6$ redox couple is used in the BPMED end compartments to replace the HER and OER, thereby avoiding the high energy consumption associated with gas evolution.

BPMED-BS system. Energy storage is achieved using a battery energy storage system, which potentially offers a higher round-trip efficiency than hydrogen-based storage. The BPMED cell configuration in this system is identical to that of the BPMED-EL-PEMFC system, adopting redox-coupled reactions in the end compartments to minimize extra voltage losses.

DAC is achieved through the pH-swing of a carbonate/bicarbonate solution within a regeneration loop, as shown in Fig. 1B. In parallel, Fig. 1C illustrates the changes in dissolved inorganic carbon (DIC) and total alkalinity (TA). The process comprises four steps (solution nodes numbered): solution basification ($4 \rightarrow 1$), atmospheric CO_2 absorption by the basified solution ($1 \rightarrow 2$), solution acidification ($2 \rightarrow 3$), and CO_2 degassing from the acidified solution ($3 \rightarrow 4$). The chemical reactions and equilibria in the solution are:[55]

$$CO_3^{2-} + H_2O \rightleftharpoons HCO_3^- + OH^- \quad (1)$$

$$HCO_3^- \rightleftharpoons CO_2(aq) + OH^- \quad (2)$$

$$H_2O \rightleftharpoons H^+ + OH^- \quad (3)$$

$$CO_2(g) \rightleftharpoons CO_2(aq) \quad (4)$$

As shown in Fig. 1B, the basification and acidification processes take place in the basic and acidic compartments of the electrochemical cell, which are separated by BPMs and cation exchange membranes (CEMs). BPMs split water into OH^- and H^+ ions without gas evolution, creating a pH difference between compartments. CEMs permit only K^+ ion crossover (H^+ crossover is negligible due to its low concentration in the carbonate/bicarbonate solution[44]), preventing acid–base neutralization and preserving the pH gradient. Each BPM unit consists of a BPM and a CEM and is repeated within a single cell.

As shown in Fig. 1C, the TA of the solution increases during the basification step and decreases during acidification, while the DIC remains constant due to the closed-system condition within the BPMED cells. In contrast, the CO_2 absorption and degassing processes occur under open-system conditions, allowing CO_2 content exchanges between solution and environment. During these processes, the solution DIC varies, while TA remains unchanged. Atmospheric CO_2 absorption by the basified solution can be performed using an air contactor designed and operated by Carbon Engineering, with a plant capacity of 1 Mt-CO_2 per year.[22] The degassing process is assumed to achieve complete equilibrium under atmospheric pressure conditions.

Table 1 Ion/solute concentrations of the regenerative carbonate/bicarbonate solution

			Ion/solute concentration (M)					
Solution	pH	DIC (M)	K^+	H^+	OH^-	CO_3^{2-}	HCO_3^-	CO_2 (aq)
① Basified solution	14.00	1.01	3.02	1.00×10^{-14}	1.00	1.01	2.16×10^{-4}	4.83×10^{-12}
② Loaded solution	11.64	1.54	3.02	2.27×10^{-12}	4.40×10^{-3}	1.47	7.16×10^{-2}	3.64×10^{-7}
③ Acidified solution	6.58	1,54	0.98	2.58×10^{-7}	3.88×10^{-8}	1.78×10^{-4}	9.79×10^{-1}	5.65×10^{-1}
④ Degassed solution	7.80	1.01	0.98	1.55×10^{-8}	6.43×10^{-7}	2.93×10^{-3}	9.73×10^{-1}	3.39×10^{-2}

The extent of the pH swing directly governs DAC performance, as a sufficiently large pH gradient is essential for establishing the chemical equilibrium required for efficient CO_2 absorption and desorption. However, a larger pH swing increases energy consumption and may reduce membrane longevity. To determine a reasonable amplitude, the basified pH is set at 14 (SI 1), which is also comparable to the absorbent condition (1 M KOH[22]) by Carbon Engineering's pilot DAC plant. Based on a prior air contactor model,[56] an absorption ratio (actual absorbed CO_2 *vs.* equilibrium capacity) of 0.9 is considered feasible. For this study, the regeneration solution has a total K^+ concentration of 2 M, and the corresponding acidified pH is 6.59. Table 1 summarizes the detailed pH, dissolved inorganic carbon (DIC), and ion concentrations derived from equilibrium eqn (1)–(4) and the assumed CO_2 absorption ratio.

Mathematical models for the BPMED cells, PV panels, electrolyzer, PEMFC, and battery system are developed (SI 2). An electrochemical model is employed to predict the voltage–current behavior and power consumption of the BPMED cells and is validated through experimental data (SI 3). Auxiliary power consumption (*e.g.*, air fans, solution pumping, and CO_2 and hydrogen gas pressurization) is neglected, as it accounts for a relatively small portion (<5%) of the total energy consumption and cost compared to BPMED cells.[44] To simplify the sizing of energy storage systems, constant energy-conversion efficiencies are assumed for the storage-related modules (electrolyzer, PEMFC, and battery). Solar energy is assumed to be fully utilized for PV electricity generation, without any curtailment. Simultaneously, system operation assumes an overall energy balance for the storage subsystems over the analysis period, meaning the final energy stored equals the initial amount. Consequently, the system simulation can be focused on determining the feasible scale of BPMED stack (n_{cell}) under specified solar energy input conditions. The number of BPMED cells is determined iteratively based on the overall energy balance from which the corresponding DAC output is derived. The detailed methodology for system operation and simulation is provided in SI 4.

System daily energetic characteristics

The systems are first simulated over a single day to evaluate their fundamental operating characteristics and DAC performance under diurnal solar variability. This daily analysis represents a strict off-grid baseline, in which all electricity demand is met solely by on-site PV generation and internal energy storage, without any grid electricity supply. Apart from location, day-to-day solar conditions are influenced by stochastic weather variability. To represent an averaged and typical diurnal pattern, an hourly solar irradiance model based on a Gaussian distribution (SI 2.2) is employed, parameterized by date, latitude, and peak irradiance. For the daily simulations, the date and latitude are set to July 1st and 22.6 °N, respectively, with a peak irradiance of 600 W m^{-2}. To keep the same energy input for all systems, the total effective area of the PV power plant is set as 1 km^2 for all cases. Table 2 summarizes key system parameters, with definitions and implementation details provided in SI 2.

There is a minimum requirement for the BPMED current density. At low current densities (<1 mA cm^{-2}), over 20% of the current through the BPMs is attributed to ion crossover rather than water dissociation.[47] To maintain high faradaic efficiencies for water dissociation (>95%), the BPMED stack should operate

Table 2 System basic parameters and assumptions

Module	Parameter	Value
PV plant	Total effective area	1 km^2
	Efficiency	18.8% (ref. 57)
	Temperature coefficient	−0.39% K^{-1} (ref. 57)
BPMED system	Average current density	10 mA cm^{-2}
	Number of BPM units in a cell (n_{BPM})	10 (redox-couple cell); 1 (HER/OER cell)
	Single membrane area	210 cm^2 (ref. 39)
	Thickness of compartments	480 μm (ref. 41)
Electrolyzer (alkaline water)	Energy efficiency	80% (ref. 58)
PEMFC	Energy efficiency	50% (ref. 59)
Battery system	Charging efficiency	95% (ref. 60)
	Discharging efficiency	95% (ref. 60)

above 5 mA cm^{-2}.[47] For simulations over a typical day, an average operating density of 10 mA cm^{-2} (as shown in Table 2) is assumed to ensure effective water dissociation for pH swing while reducing extra ohmic losses.

In the BPMED-EL-PEMFC and BPMED-BS systems, where the energy production for storage is decoupled from the BPMED stack (*via* the electrolyzer or battery), the distribution between direct supply and energy storage can be flexibly adjusted, as shown in Fig. 1A. Under the off-grid assumption, this flexibility enables the BPMED stack to operate at a constant current density of 10 mA cm^{-2} throughout the day. In contrast, the BPMED-PEMFC system lacks a separate energy production module to divert excess PV electricity; consequently, its current density passively follows PV generation during daylight hours. For consistency, the average current density over the daily cycle is maintained at 10 mA cm^{-2} across all systems.

The number of repetitive BPM units in single cells is also a critical factor for the BPMED stacks. In the HER/OER cell configuration, increasing the number of BPM units effectively dilutes the energy input across more units, thereby reducing the energy available for hydrogen and oxygen evolution in the end compartments. This results in reduced energy storage, which noticeably amplifies the passive fluctuation in current density throughout the day (Fig. S6). To minimize such fluctuation and better match with the constant current condition of the other two systems, the HER/OER cell configuration employs a single BPM unit ($n_{BPM} = 1$). In contrast, in the redox-couple cell configuration, increasing the number of BPM units within a single cell can reduce the average energy consumption of the redox reaction compartments. However, the benefit of adding more BPM units (*e.g.* from 10 to 100) could be marginal, while using fewer units offers advantages in assembly simplicity and operational uniformity across compartments. To balance the energy efficiency and the structural complexity, the redox-couple cell configuration with 10 BPM units ($n_{BPM} = 10$) is considered reasonable and adopted. The detailed calculation and discussion can be found in SI 5.

Fig. 2A and B shows the daily profiles of BPMED current density and component power consumption across the systems. As explained above, in the BPMED-PEMFC system, the current density passively fluctuates with solar radiation during the daytime, and Fig. 2A exhibits a varying range of 5.6–21.7 mA cm^{-2} (with an average of 10 mA cm^{-2}). At night, in the absence of solar input, the hydrogen generated by the HER compartment is consumed and sustains a steady current density of 5.6 mA cm^{-2}. This level of fluctuation remains acceptable, as the

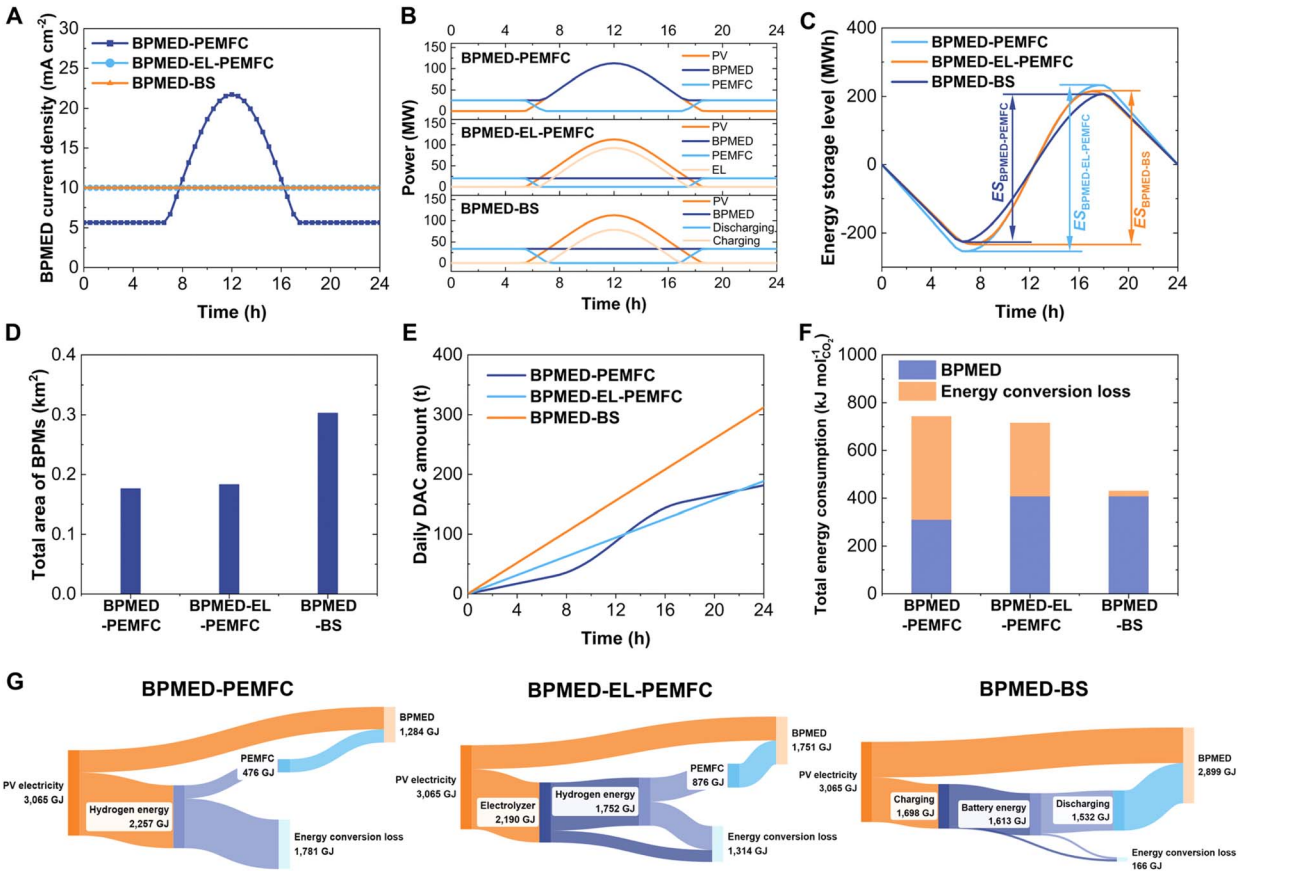

Fig. 2 Performance comparison of DAC systems over a typical day powered by 1 square kilometre of PV input. (A) BPMED operating load (current density) variations. (B) Daily power distribution and variations across system components. (C) Net energy storage level fluctuations, highlighting storage requirements. (D) Total BPMED stack size (reflected by the BPM area) for each system. (E) Daily DAC amount. (F) Total energy consumption for DAC. (G) Energy flow diagrams showing input, storage, utilization, and conversion losses.

minimum current density suffices for BPM water dissociation, while the maximum is only approximately twice the average. Although the integrated hydrogen production in the HER/OER configuration does not fully stabilize the BPMED power supply, it helps prevent nighttime shutdown and frequent on–off cycling of the stack and DAC processes. In contrast, the BPMED-EL-PEMFC and BPMED-BS systems, equipped with electrolyzer and battery systems, maintain a constant BPMED current density of 10 mA cm^{-2}, as shown in Fig. 2A. Their power consumption fluctuates within 0–93 MW and 0–79 MW, respectively, enabling full utilization of excess PV electricity during daylight hours, as shown in Fig. 2B. The BPMED stack power in these two systems remains stable at 20.27 MW and 33.56 MW throughout the day, whereas it varies between 25.47 MW and 112.8 MW in the BPMED-PEMFC system. Overall, while all configurations are operationally feasible, the BPMED-EL-PEMFC and BPMED-BS systems offer better stability for continuous BPMED and DAC operation.

Assuming an initial energy storage level of 0, Fig. 2C illustrates its variation throughout the day. The hydrogen energy content is calculated using its high heating value. The imposed daily energy balance ensures that the final storage level returns to 0, confirming that all electricity demand is met internally by PV generation and storage, without reliance on external power supply. The difference between the peak and trough values represents the required energy storage capacity. In the BPMED-PEMFC system, the passive fluctuation of BPMED power reduces the storage demand, resulting in the lowest requirement of 432 MWh among the three systems. For the BPMED-EL-PEMFC and BPMED-BS systems, the corresponding values are 487 MWh and 448 MWh, respectively. The BPMED-BS system requires less storage than the BPMED-EL-PEMFC system, primarily because of the battery's higher energy-releasing efficiency (95%). By comparison, the PEMFC delivers only 50% of the stored hydrogen energy as electricity, requiring greater storage to sustain constant BPMED power. Nevertheless, the differences among the three systems remain within 15% over the one-day simulation, indicating a relatively minor impact on the overall energy storage burden.

Under identical solar energy input and PV power from a 1 km^2 PV plant, the feasible BPMED stack scale (reflected by the BPM area) is compared across the three systems in Fig. 2D. The total BPM area in the BPMED-BS system reaches 0.33 km^2, which is 71.9% and 65.5% larger than that of the BPMED-PEMFC system and BPMED-EL-PEMFC system, respectively. This indicates a significantly larger feasible BPMED stack scale, which also translates into a higher DAC capacity. Since the average current density is maintained at a consistent level across all systems, the DAC productivity per unit BPM area remains similar, making the total one-day DAC amount directly proportional to the total BPM area. As shown in Fig. 2E, the BPMED-BS system achieves a DAC productivity of 312 t by the end of the day, exceeding the other two systems by exactly the same percentages as in BPM area. These results indicate that the BPMED-BS system exhibits superior solar energy utilization efficiency compared to the hydrogen-storage-based systems. Moreover, the nearly identical BPMED stack scales and daily DAC capacities of the BPMED-PEMFC and BPMED-EL-PEMFC systems suggest comparable overall energy utilization efficiencies, regardless of whether hydrogen is produced *via* a separate electrolyzer or integrated HER compartments in BPMED cells.

The systems' overall energy consumption, expressed as the specific DAC amount, is compared in Fig. 2F. Notably, the BPMED-BS system achieves the lowest DAC energy consumption of 430 kJ per mol-CO_2. In comparison, the two hydrogen-storage-based systems exhibit energy consumption exceeding 700 kJ per mol-CO_2. The superior energy efficiency of the BPMED-BS system is attributed to the high round-trip efficiency of its battery storage system (90%). In contrast, the lower round-trip efficiency of the electrolyzer and PEMFC systems (40%) results in significantly greater energy losses during conversion, as reflected in Fig. 2F.

Fig. 2G further provides a detailed comparison of energy flows across the systems throughout the day. The streams of energy loss represent conversion losses during energy storage and utilization. In the BPMED-BS system, the energy loss from battery storage accounts for only 5.4% of the total input PV electricity, highlighting the high efficiency of this approach. In contrast, the BPMED-PEMFC system allocates 73.6% of the total energy to hydrogen production, as its built-in hydrogen generation is coupled with BPMED, and must operate continuously throughout the day. This leads to the highest energy conversion losses of 58.1% among the systems. However, as shown in Fig. 2F, the BPMED efficiency of the HER/OER cell is higher than that of the redox-couple cell. This is primarily due to the lower current density and reduced potential loss during nighttime operation. Consequently, the total DAC energy consumption of the BPMED-PEMFC system is comparable to that of the BPMED-EL-PEMFC system. In summary, the battery energy storage strategy demonstrates significantly higher energy efficiency compared to the hydrogen-based storage strategies.

Global assessment of annual off-grid operation

Accounting for seasonal environmental conditions, the simulation period is extended to one year to evaluate the systems' annual performance and economic outcomes under off-grid operation. In addition to representative site-level case studies, a spatially resolved assessment is performed to capture geographic heterogeneity in solar resource availability and its impact on DAC cost. Specifically, two illustrative locations: Shenzhen, China (22.6 °N, 114.0 °E, Fig. 3) and North East Scotland, UK (56.1 °N, 3.3 °E, Fig. 4), are selected to represent low- and high-latitude deployment scenarios, respectively. These site-level analyses are complemented by a country-scale assessment using 50 representative locations across China and 50 across the UK, enabling systematic evaluation of spatial variability in solar-driven DAC performance (Fig. 5).

Fig. 3A and 4A show the annual variations in solar irradiance and ambient temperature for Shenzhen and North East Scotland,[61] respectively, providing a baseline for seasonal system behavior. The total DAC cost includes both capital expenditure

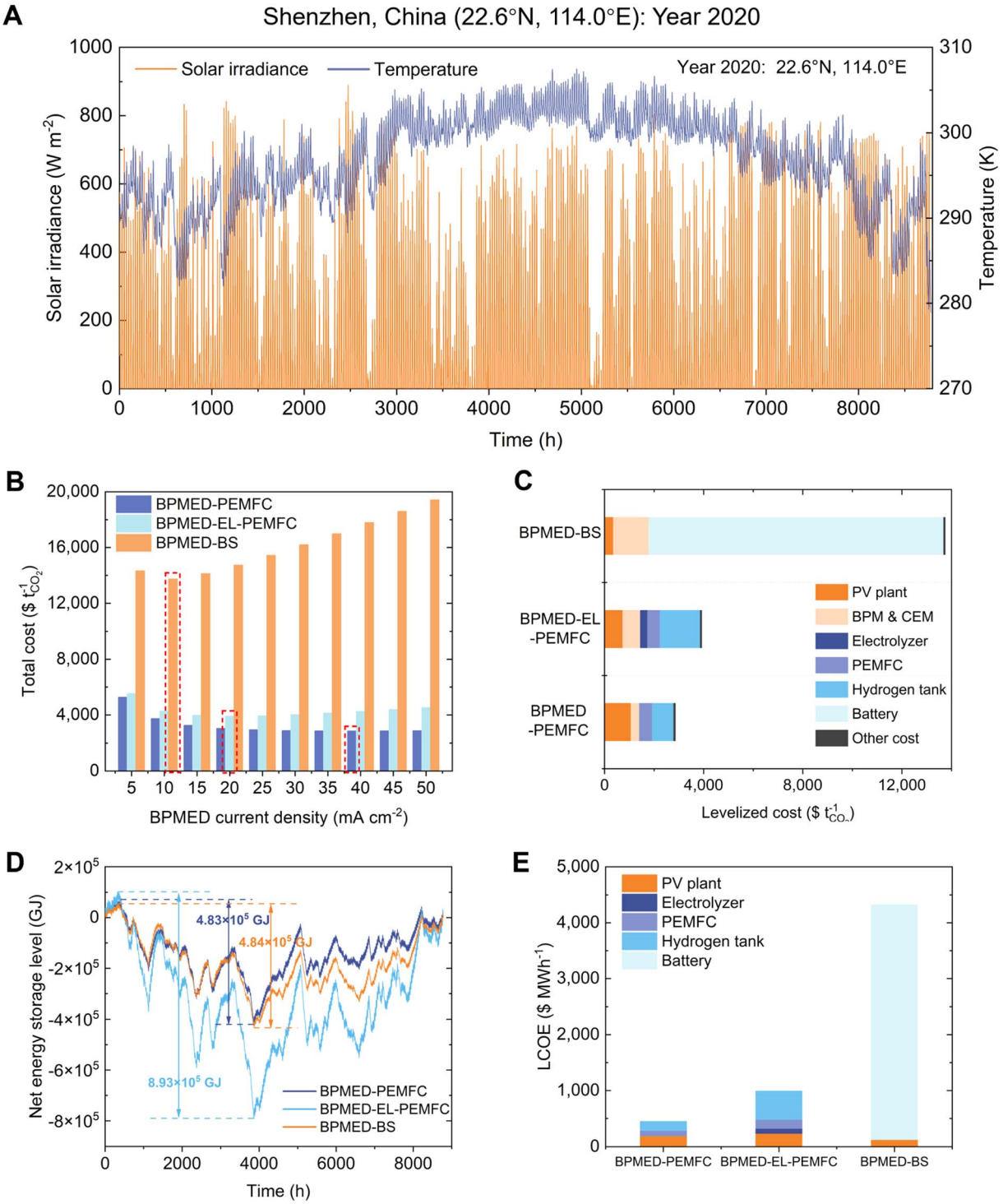

Fig. 3 Economic performance of systems for the Shenzhen case. (A) Annual variations in solar irradiance and temperature. (B) Impact of current density on DAC total cost. (C) Cost breakdown at the optimal point. (D) Profiles of energy storage amount and required capacity. (E) LCOE of energy production and storage.

and operation and maintenance (O&M) costs. Detailed calculation methods and assumptions are provided in SI 6.

As previously discussed, the scales of the BPMED stack and energy storage systems are primarily determined by the available PV output and the average BPMED operating current density. For each location, one-year operational simulations are conducted over a range of BPMED current densities, initially assuming a PV area of 1 km^2. System components are then proportionally scaled to achieve an annual DAC capacity of 1 Mt-CO_2, and the optimal current density is identified by minimizing the total DAC cost.

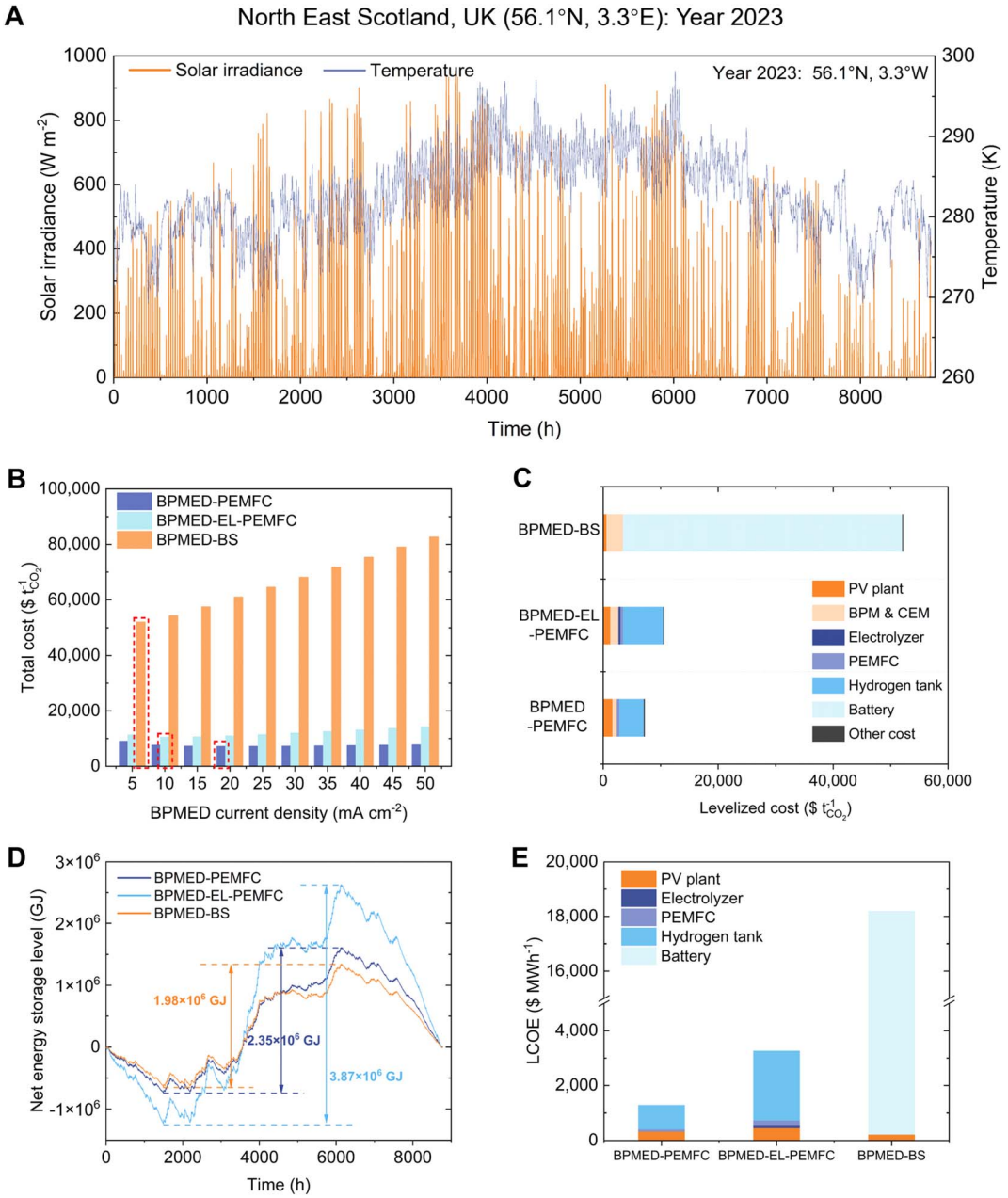

Fig. 4 Economic performance of systems for the North East Scotland case. (A) Annual variations in solar irradiance and temperature. (B) Impact of current density on DAC total cost. (C) Cost breakdown at the optimal point. (D) Profiles of net energy storage amount and required capacity. (E) LCOE of energy production and storage.

As the average BPMED current density varies from 5 to 50 mA cm^{-2}, the corresponding DAC total costs for all systems are evaluated and presented in Fig. 3B and 4B. In the BPMED-EL-PEMFC and BPMED-BS systems, the BPMED current density remains constant over the entire simulation period, whereas in the BPMED-PEMFC system, it passively fluctuates in response to the PV output. The fluctuation range of current density and detailed sizes of the other components are detailed in Table 3. For the Shenzhen case, the optimal average BPMED current densities (corresponding to the minimum total DAC costs) are identified as 40, 20, and 10 mA cm^{-2} for the BPMED-PEMFC, BPMED-EL-PEMFC, and BPMED-BS systems, respectively, as highlighted in Fig. 3B. In contrast, for the North East Scotland case, the optimal values are lower, at 20, 10, and 5 mA cm^{-2}, respectively. These differences reflect the influence of local solar irradiance conditions on system operation and optimal design.

Overall, a comparison of Fig. 3B and 4B reveals that the total DAC costs for all system configurations are substantially lower in the Shenzhen case. The BPMED-PEMFC system yields the lowest total cost at 2849 \$ per t-CO_2, while the BPMED-BS system incurs the highest optimum cost of 13 746 \$ per t-CO_2. The BPMED-EL-PEMFC system falls in between, with an optimum cost of 3919 \$ per t-CO_2. In North East Scotland, the corresponding values increase to 7189 \$ per t-CO_2, 52 135 \$ per

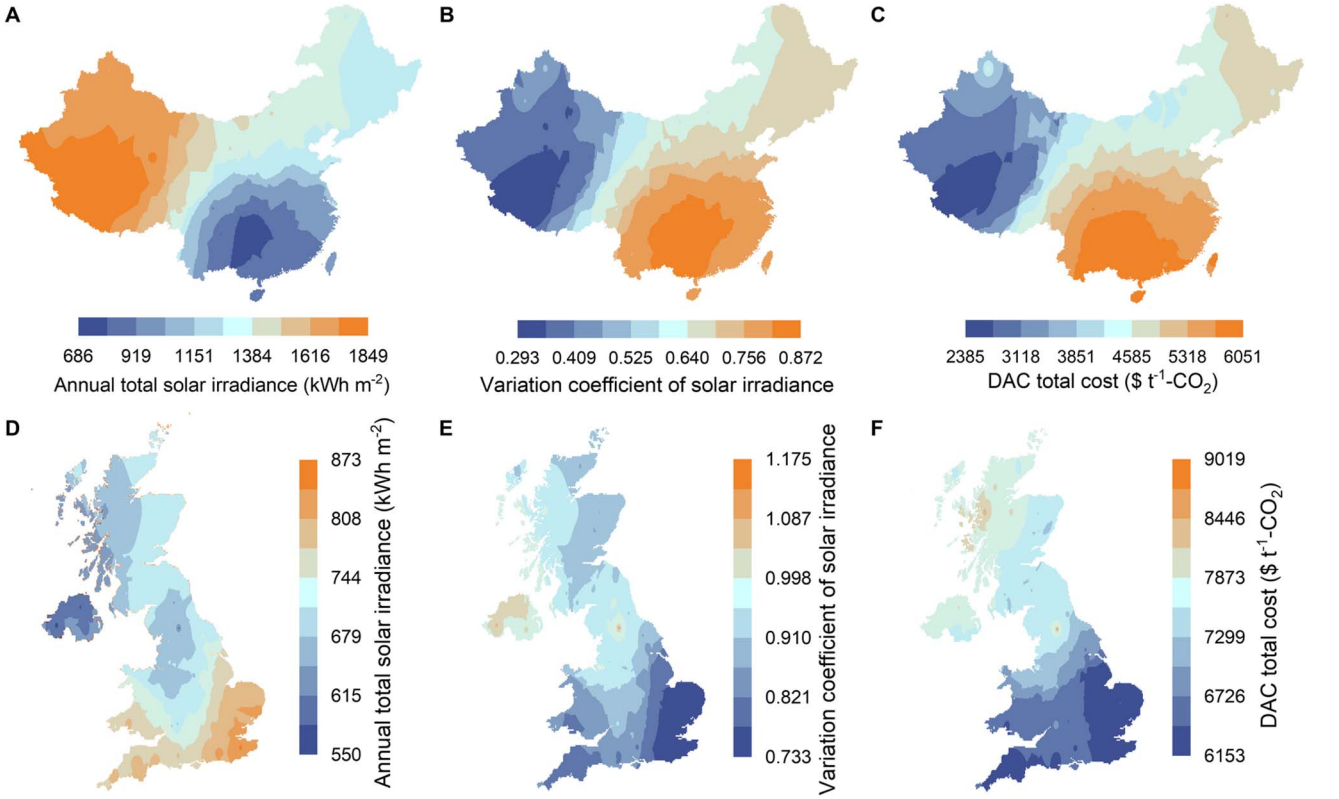

Fig. 5 Regional comparison of the solar irradiance condition and optimal off-grid DAC cost based on the BPMED-PEMFC system. China (based on year 2020 solar irradiance data): (A) annual total solar irradiance; (B) variation coefficient of daily solar irradiance; (C) optimal DAC total cost. UK (based on year 2022 solar irradiance data): (D) annual total solar irradiance; (E) variation coefficient of daily solar irradiance; (F) optimal DAC total cost.

t-CO_2 and 10 556 $ per t-CO_2, respectively, representing cost escalations exceeding 152%. These results highlight the dominant influence of local solar irradiance condition on system economic performance. Moreover, even in the favorable Shenzhen case, the lowest total cost of 2849 $ per t-CO_2 still remains considerably higher than the cost benchmarks reported for existing DAC plants.

To identify the dominant contributors to the high total cost, the detailed breakdown of optimized total costs for all systems is shown in Fig. 3C and 4C for the Shenzhen and North East Scotland cases, respectively. In the Shenzhen scenario, energy storage components (hydrogen tank and PEMFC) account for 48% of the total cost in the BPMED-PEMFC system, representing the lowest energy storage cost share among the three systems. Meanwhile, the energy storage-related costs (electrolyzer, hydrogen tank, PEMFC, and battery) comprise 62% and 87% of the total cost in the BPMED-EL-PEMFC and BPMED-BS systems respectively. By contrast, the costs of other fundamental system components (PV panels, BPMED cell materials, and the air contactor) remain relatively consistent and within an acceptable range, between 1400 and 1800 $ per t-CO_2 in the Shenzhen case. In North East Scotland, the cost contribution from energy storage becomes even more pronounced. Notably, in the BPMED-BS system, the battery alone accounts for 93% of the total cost. These high proportions

Table 3 Optimized system sizing for 1 Mt-CO_2 per year DAC

	Shenzhen (22.6 °N, 114.0 °E)			North East Scotland (56.1 °N, 3.3 °E)		
Parameters	BPMED-PEMFC	BPMED-EL-PEMFC	BPMED-BS	BPMED-PEMFC	BPMED-EL-PEMFC	BPMED-BS
Total PV area (km^2)	35.97	26.20	12.87	58.81	45.57	21.87
Total BPM area (km^2)	0.66	1.33	2.65	1.33	2.65	5.30
Current density (mA cm^{-2})	17.6–161.3 (average 40)	20	10	7.8–150.9 (average 20)	10	5
Electrolyzer scale (MW)	N.A.	1570	N.A.	N.A.	1803	N.A.
PEMFC scale (MW)	331	326	N.A.	274	2854	N.A.
Hydrogen storage scale (t)	3404	6294	N.A.	16 581	27 279	N.A.
Battery storage scale (GWh)	N.A.	N.A.	135	N.A.	N.A.	549

highlight the substantial economic burden associated with energy storage.

In addition, compared to the PEMFC and electrolyzer, the costs of the hydrogen tank and battery are more significant. It is therefore important to examine the underlying factors that necessitate such large-scale energy storage components. Fig. 3D and 4D present the annual profiles of energy storage levels for the three systems. The required capacities of hydrogen tanks and batteries are dictated by the difference between the annual peak and valley energy storage levels. In addition to minor fluctuations caused by the daily solar cycle, pronounced seasonal variations are observed, leading to significant differences between peak and valley values. For the Shenzhen case, the energy storage requirements for the BPMED-PEMFC, BPMED-EL-PEMFC, and BPMED-BS systems are 4.83×10^5, 8.93×10^5, and 4.84×105 GJ, respectively. Moreover, the corresponding storage capacities required in the North East Scotland case are substantially higher, increasing by approximately a factor of four. These large-scale energy storage demands span weeks to months, becoming the primary drivers behind the high associated costs of the storage subsystems.

As discussed in the typical-day analysis, battery storage is more energy efficient in electrochemical DAC systems. Its high round-trip efficiency makes it well-suited for short-term energy storage and conversion. However, for long-term off-grid operation requiring large-scale energy storage over weeks or months, battery storage becomes economically less favorable compared to hydrogen storage. In the Shenzhen case, the battery cost in the BPMED-BS system reaches 11 901 \$ per t-CO_2, directly rendering it the most expensive configuration in terms of DAC total cost. In contrast, the hydrogen tank costs are substantially lower, at 867 \$ per t-CO_2 and \$1619 \$ per t-CO_2 in the BPMED-PEMFC and BPMED-EL-PEMFC systems, respectively. As storage capacity scales, hydrogen tanks provide a lower cost per unit of energy stored compared to expanding battery capacity. A hybrid configuration may therefore offer a promising solution, with batteries managing short-term variability and hydrogen storage addressing long-duration energy balancing. Such an approach could mitigate the high economic burden associated with energy storage in off-grid electrochemical DAC systems.

A closer examination of the relationship between energy storage levels and solar irradiance distribution reveals a strong correlation. In the Shenzhen case, for example, a period of low solar irradiance can be observed between approximately 3300 h and 3900 h in Fig. 3A, likely corresponding to consecutive overcast or cloudy days. This period coincides with a sharp decline in net energy storage levels, as shown in Fig. 3D. In the BPMED-EL-PEMFC system, the net energy storage level for the entire system (with 1 Mt-CO_2 per year DAC capacity) decreases from approximately -3×10^5 GJ to -8×10^5 GJ, reaching its annual minimum. Similarly, in the North East Scotland case, solar irradiance is more concentrated between 3400 h and 4100 h, as well as between 5500 h and 6100 h, as shown in Fig. 4A. During these intervals, the net energy storage in the BPMED-EL-PEMFC system consistently increases from approximately 7×10^5 GJ to 2.7×10^6 GJ, reaching the highest level of the year, as shown in Fig. 4D. These observations highlight the decisive impact of short-term weather variability on fluctuations in energy storage level. Meanwhile, a comparison of the general profile trends in Fig. 3D and 4D reveals no consistent pattern in the timing of these fluctuations. Such variability and uncertainty significantly increase the required scale of energy storage infrastructure, thereby driving a notable rise in DAC total costs.

As shown in Fig. 4A and D, the higher-latitude location of North East Scotland exhibits a markedly more uneven solar irradiance distribution throughout the year, resulting in greater amplitude fluctuations in energy storage levels. This is the primary driver behind the significantly larger energy storage requirements and higher system costs compared to Shenzhen. Moreover, the lower solar resource availability in North East Scotland necessitates larger PV arrays and BPMED stacks to achieve the same annual DAC target of 1 Mt-CO_2. From Table 3, the effective PV area for the three systems increases from 35.97, 26.20, and 12.87 km^2 in Shenzhen to 58.81, 45.57, and 21.87 km^2 in North East Scotland, respectively. The increasing rates are over 60%. Correspondingly, the BPMED stack scale (total BPM area) in North East Scotland is approximately double that required in Shenzhen. These factors contribute to higher costs not only for energy storage but also for the other core system components. The comparison between the two cases highlights the critical influence of geographic location on the economic performance of PV-powered DAC systems.

Beyond these representative sites, Fig. 5 further provides a country-scale spatial comparison of annual total solar irradiance, the coefficient of daily solar irradiance variation (defined in SI 7), and the corresponding optimal off-grid DAC total cost across China and the UK. The detailed data are provided in SI 8. Fig. 5A and D show that annual solar irradiance exhibits strong geographic gradients in both countries, with substantially higher values in western China and lower values across most regions of the UK. Fig. 5B and E further reveal pronounced spatial heterogeneity in the temporal uniformity of solar resources, as quantified by the variation coefficient of daily irradiance. Regions with lower variation coefficients exhibit more evenly distributed daily solar input over the year, whereas higher coefficients indicate stronger intermittency and clustering of solar availability.

The combined influence of solar magnitude and temporal uniformity is reflected in the spatial distribution of optimal off-grid DAC total cost shown in Fig. 5C and F. In China, optimal off-grid DAC costs span approximately 2300–6000 \$ per t-CO_2 across the 50 representative sites (Fig. 5C). Lower-cost regions are predominantly located in southern and central China, where relatively high annual solar irradiance (exceeding 1300 kWh m^{-2}) is coupled with moderate day-to-day variability (variation coefficients below 0.5). In contrast, the spatial cost distribution in the UK (Fig. 5F) is shifted to substantially higher values, ranging from approximately 6000 to 9000 \$ per t-CO_2. This increase reflects both lower annual irradiation (generally below 900 kWh m^{-2}) and higher temporal variability (variation coefficients exceeding 0.8) across most regions. Although southern and eastern England benefit from comparatively higher solar input and lower variability than Scotland and western regions, even the most favorable UK locations remain

significantly more costly than typical Chinese sites under strict off-grid operation. This again emphasizes the profound geographic dependence of solar-driven DAC feasibility and suggests that deployment strategies must be tailored to regional resource characteristics.

Across both countries, regions characterized by high annual solar irradiance and low daily variability consistently exhibit lower DAC costs. This trend demonstrates that DAC cost is not determined by annual solar resource alone, but by the joint effect of energy availability and temporal consistency, which together govern the required scale of PV generation and long-duration energy storage. This observation further generalizes the trends identified at the two representative sites, linking solar irradiance distribution to seasonal energy-storage fluctuations and overall system cost. These findings reinforce the importance of siting optimization for renewable-powered DAC systems and suggest that, in many regions, purely off-grid operation may face prohibitive economic penalties. This motivates the exploration of hybrid deployment and power supply strategies, including DAC load flexibility and grid-assisted operation.

The influence of solar conditions on system total cost is manifested primarily through their impact on required generation capacity and long-duration energy storage infrastructure, which together can be quantitatively captured by the levelized cost of electricity (LCOE). The LCOE is therefore calculated to isolate the economic performance of renewable electricity supply for the proposed off-grid systems. In this assessment, only the electricity ultimately delivered to the BPMED stacks is considered, excluding losses incurred during energy storage and conversion processes. Meanwhile, only the costs associated with energy components (PV plant, electrolyzer, PEMFC, hydrogen tank, and battery) are included in the calculation. The resulting LCOEs and their cost breakdowns for both locations are shown in Fig. 3E and 4E, respectively. In the Shenzhen case, the LCOEs are 447, 991, and 4324 \$ MWh^{-1} for the BPMED-PEMFC, BPMED-EL-PEMFC, and BPMED-BS systems, respectively. These values increase significantly in the North East Scotland case, reaching 1,276, 3,257, and 18 186 \$ MWh^{-1}, respectively. The energy storage components still contribute the majority share in the LCOEs. In this regard, Weinand *et al.*[62] report that the LCOEs for decentralized off-grid renewable energy systems globally range between 30 and 1000 \$ MWh^{-1}, with an average of 290 \$ MWh^{-1}. The values reported in this study are thus relatively high. This is likely attributable to the absence of system optimization strategies, such as curtailment management and the integration of complementary renewable sources (*e.g.*, wind) to improve the capacity factor and smooth supply fluctuations. Achieving more affordable DAC powered by renewable electricity will require substantial LCOE reductions, which may be facilitated by further improvement in system configurations and operating strategies.

Effect of operational and electricity flexibility

The annual and spatial analyses above reveal that the economic performance of off-grid electrochemical DAC is fundamentally constrained by long-duration energy storage requirements. We further investigate whether these constraints can be alleviated through a combination of flexible BPMED operation and grid-assisted electricity supply. The case of Shenzhen is selected as the baseline for further discussion.

As shown in Table 3, the BPMED current density in the BPMED-PEMFC system varies by approximately one order of magnitude in both Shenzhen and North East Scotland, indicating substantial operational flexibility. By contrast, the BPMED-EL-PEMFC and BPMED-BS systems maintain a constant current density throughout the year. This discrepancy introduces unfairness for direct cost comparison, as the BPMED-PEMFC system benefits economically from inherent load flexibility. Nonetheless, enabling flexible-load operation in the BPMED stacks of the other two systems could serve as an effective strategy to reduce the energy storage demand. By dynamically adjusting current density in accordance with PV electricity output, the need for long-duration storage could be significantly alleviated, potentially leading to further reductions in DAC total cost.

The lower and upper limits of BPMED current density are set between 5 and 100 mA cm^{-2} to evaluate the effect of flexible-load operation in the BPMED-EL-PEMFC and BPMED-BS systems under the Shenzhen scenario. The corresponding variations in DAC total cost are presented in Fig. 6A and B, respectively. The *x*- and *y*-axes represent the lower and upper bounds of BPMED current density, respectively, with the evaluated variation ranges confined to the upper-left triangular region of each plot. The closer to the upper-left corner, the greater the fluctuation range in BPMED current density, while the diagonal line represents constant-load operation.

As discussed previously, the minimum DAC total costs for the BPMED-EL-PEMFC and BPMED-BS systems under constant-load operation are 3919 and 13 746 \$ per t-CO_2, respectively. Under the widest evaluated fluctuation range (5 to 100 mA cm^{-2}), these values are reduced by over 50%, to 1892 and 5845 \$ per t-CO_2, respectively. According to Table 3, the BPMED current density in the BPMED-PEMFC system varies between 17.6 and 161.3 mA cm^{-2}, representing a fluctuation of approximately nine-fold. Within a comparable fluctuation range of 10–90 mA cm^{-2}, the total costs of the BPMED-EL-PEMFC and BPMED-BS systems drop to 2163 and 7998 \$ per t-CO_2, respectively. Compared to the BPMED-PEMFC system's minimum cost of 2849 \$ per t-CO_2, these results indicate that the BPMED-EL-PEMFC system can achieve lower total costs under similar flexible-load conditions. Although the BPMED-BS system still exhibits higher total costs than the BPMED-PEMFC configuration, it nonetheless benefits substantially from load flexibility.

Fig. 6C presents profiles of energy storage level under different BPMED current density fluctuation ranges. It is evident that wider fluctuation ranges lead to reduced variations in energy storage levels, thereby lowering the required capacities of energy storage components. Nevertheless, while more flexible BPMED operation effectively reduces both the energy storage and total costs, it may introduce challenges related to system stability and operational feasibility. Further technical investigation is essential to evaluate the practicality and long-

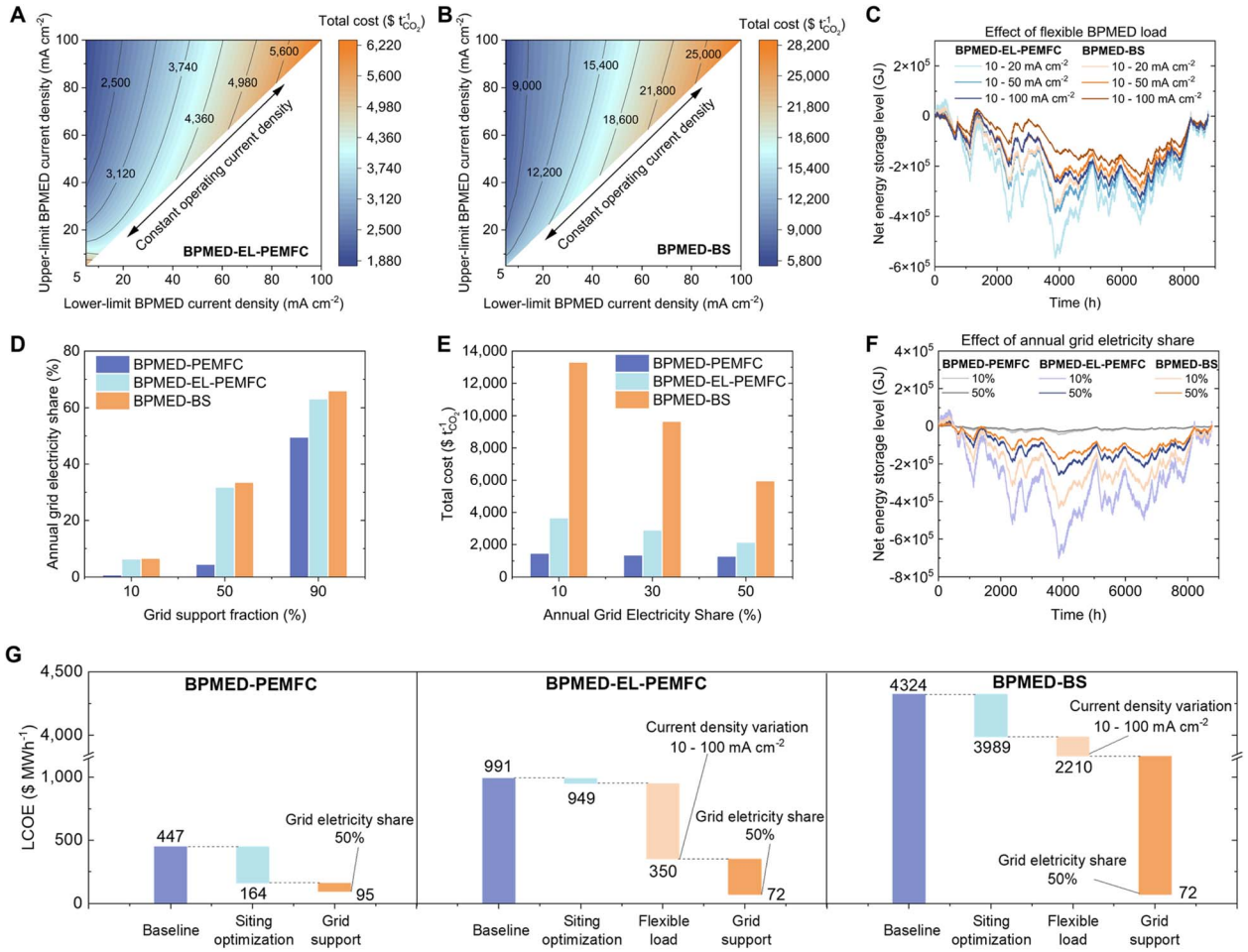

Fig. 6 Effect of flexible BPMED current density and grid electricity support on system performance. (A) Variation in total cost of the BPMED-EL-PEMFC system under variable BPMED current density. (B) Variation in total cost of the BPMED-BS system under variable BPMED current density. (C) Annual profiles of net energy storage level under different BPMED current density fluctuation ranges. (D) Relation between grid support fraction and annual grid electricity share. (E) Effect of grid electricity supply on the system total cost. (F) Annual profiles of net energy storage level under different grid electricity share conditions. (G) The LCOE reduction paths of the three proposed systems.

term reliability of implementing such flexible-load strategies in actual deployments. Additionally, while flexible BPMED operation helps mitigate seasonal fluctuations in energy storage level, it does not eliminate them entirely. In the BPMED-BS system, large seasonal storage requirements persist even under wide current-density fluctuation ranges, leaving battery cost as the dominant contributor to the total DAC cost. This indicates that operational flexibility addresses but does not resolve the structural limitations imposed by off-grid solar intermittency.

Fig. 6D–F extend the analysis by introducing electricity supply flexibility through grid-assisted operation. Two parameters were defined to numerically describe the extent of grid electricity supply: When the PV output power is insufficient for BPMED demand, a fraction (grid support fraction) of the power gap is filled by grid electricity, while the rest is still supplied by the stored solar energy. Over annual operation, the fraction of total grid-supplied electricity relative to the overall BPMED electricity input is defined as the annual grid electricity share. The BPMED stack is assumed to operate at a constant/average current density of 20 mA cm^{-2}, and the detailed calculation method is provided in SI 9.

Fig. 6D shows the relationship between these two parameters for the Shenzhen case. Across a wide grid support fraction range of 10–90%, the resulting annual grid electricity share remains consistently lower, varying between approximately 0.5% and 65%. To preserve PV electricity as the dominant long-term energy source, the annual grid electricity share is constrained to values below 50% in the following analysis. The impact of grid assistance on DAC total cost is summarized in Fig. 6E. Grid support leads to pronounced cost reductions, particularly for the BPMED-EL-PEMFC and BPMED-BS systems. When the annual grid electricity share reaches 50%, total DAC costs decrease to 2100 and 5914 $ per t-CO_2, respectively, while the BPMED-PEMFC system attains the lowest overall cost of 1410 $ per t-CO_2. These reductions are primarily driven by the suppression of long-duration seasonal energy-storage requirements, as reflected by the damped storage-level fluctuations shown in Fig. 6F. These results demonstrate that appropriately

limited grid-assisted electricity supply can deliver substantial cost reductions by alleviating structural storage burdens, while maintaining renewable electricity as the primary energy source for DAC operation.

Fig. 6G summarizes the combined effects of siting optimization, operational flexibility, and grid-assisted electricity supply on the achievable LCOE of the three systems. The optimal site is selected as the location with the lowest DAC total cost identified in Fig. 5C (36.089 °N, 81.422 °E). Across the three systems, the relative impact of each factor differs markedly. For example, grid assistance yields the largest LCOE reduction for the BPMED-BS system, decreasing the LCOE from 2210 to 72 \$ MWh^{-1}, whereas the largest reduction for the BPMED-EL-PEMFC system, from 949 to 350 \$ MWh^{-1}, is achieved through flexible BPMED load operation. These results further highlight the distinct operational and economic characteristics of the three proposed system configurations.

Despite the differing impacts of individual factors, the final LCOEs for all three systems are estimated to fall below 100 \$ MWh^{-1} under the most flexible operating conditions, corresponding to a BPMED current-density range of 10–100 mA cm^{-2} and an annual grid electricity share of 50%. These values define a potentially achievable lower bound for the LCOE of solar-driven energy systems, and indicate that power generation and supply costs compatible with practical deployment may be attainable under appropriately designed operating and electricity supply strategies. Correspondingly, the DAC total costs for the three systems are reduced to below 1000 \$ per t-CO_2.

Prospect of BPMED DAC under reduced electricity and material costs

Building on the preceding analysis, which identified a practical lower bound for electricity cost, this section explores the longer-term prospects of BPMED DAC under continued reductions in renewable electricity and material costs. Sustained advances in renewable electricity generation and supply strategies are expected to substantially reduce effective LCOEs in the coming decades. Potential solutions include integrating supplementary renewable energy sources,[63] deploying advanced energy storage technologies,[64] and connecting to large-scale renewable power grids to enable a more flexible and cost-effective operation.[65] Recent developments in PV electricity systems are summarized in SI 10. Combining the reported results and above LCOE lower bound estimations, the LCOEs in the range of 50–400 \$ MWh^{-1} are technically and economically feasible for reliable power delivery. This range therefore provides a realistic benchmark for assessing the future competitiveness of BPMED DAC systems.

To evaluate the economic potential of the electrochemical DAC systems under such optimized electricity costs, a simplified scenario based on the BPMED-BS system and Shenzhen case is simulated. In this analysis, the BPMED stack is assumed to operate continuously at a constant current density of 10 mA cm^{-2} throughout the year, with the LCOE fixed within the range of 50–400 \$ MWh^{-1}. Thereby, the costs of energy generation and storage components, including PV plant and battery, are excluded from cost breakdowns.

In addition to renewable electricity cost, the material costs of the electrochemical cells could be another key driver of the system total cost. As shown in Fig. 3C, for the BPMED-BS system, the cost of BPM and CEM reaches 1426 \$ per t-CO_2, substantially exceeding the corresponding PV plant cost of 361 \$ per t-CO_2. In addition, the unit cost of BPMs is estimated at 750 \$ m^{-2}, nearly an order of magnitude higher than that of CEMs.[44] As electricity costs decline, BPM price therefore emerges as a dominant economic bottleneck. Continued progress in membrane engineering is expected to alleviate this constraint over time, motivating the coupled sensitivity analysis of BPM cost and electricity price presented in this section.

In the evaluated cost range, the results demonstrate that electricity cost exerts a stronger influence than membrane cost. From Fig. 7A, with BPM cost fixed at 100 \$ m^{-2}, the DAC total cost increases more than fourfold, from 330 to 1480 \$ per t-CO_2, as LCOE increases from 50 to 400 \$ MWh^{-1}. In contrast, reducing BPM cost from 800 to 100 \$ m^{-2} lowers DAC total cost by less than half at a fixed LCOE of 200 \$ MWh^{-1}. This again highlights the central importance of continued progress in renewable electricity deployment and cost reduction to enable scalable and economically viable BPMED DAC.

In parallel, Fig. 7B further illustrates how the optimal BPMED operating current density depends on the relative importance of electricity and material costs. When electricity prices are high, lower current densities (15–35 mA cm^{-2}) are favored to reduce overpotential losses and limit energy consumption. In contrast, when membrane costs dominate, higher current densities (55–85 mA cm^{-2}) are preferred to increase pH-swing productivity per unit membrane area. This highlights a fundamental design consideration for electrochemical DAC systems: achieving stable performance at elevated current densities is essential, particularly under current conditions where membrane materials remain costly. The identified operating window of 15–85 mA cm^{-2} offers practical guidance for optimizing BPMED cell performance across a range of future economic scenarios.

Fig. 7C places these projections in the context of currently deployed DAC technologies (detailed data are provided in SI 11). Although several DAC start-ups have reported low total costs, few have released independently validated performance data. The figures disclosed by Climeworks and Carbon Engineering are considered the most reliable benchmarks. According to Keith *et al.*,[22] Carbon Engineering's high-temperature calcium-looping process achieves a total DAC cost of 94–232 \$ per t-CO_2, approaching the 100 \$ per t-CO_2 target line for large-scale deployment. In contrast, Climeworks has reported a total cost of 500–600 \$ per t-CO_2 based on their commercial plant operations. For both companies, their thermal DAC systems exhibit specific energy consumptions of within 300–400 kJ per mol-CO_2. As shown in Fig. 7C, the BPMED systems powered by PV electricity and energy storage display a broader overall energy-consumption (including energy losses in conversion and storage) range of 307–937 kJ per mol-CO_2, depending on the operating current density. The corresponding total cost currently exceeds 1800 \$ per t-CO_2, remaining several-fold higher than that of established thermal systems. However,

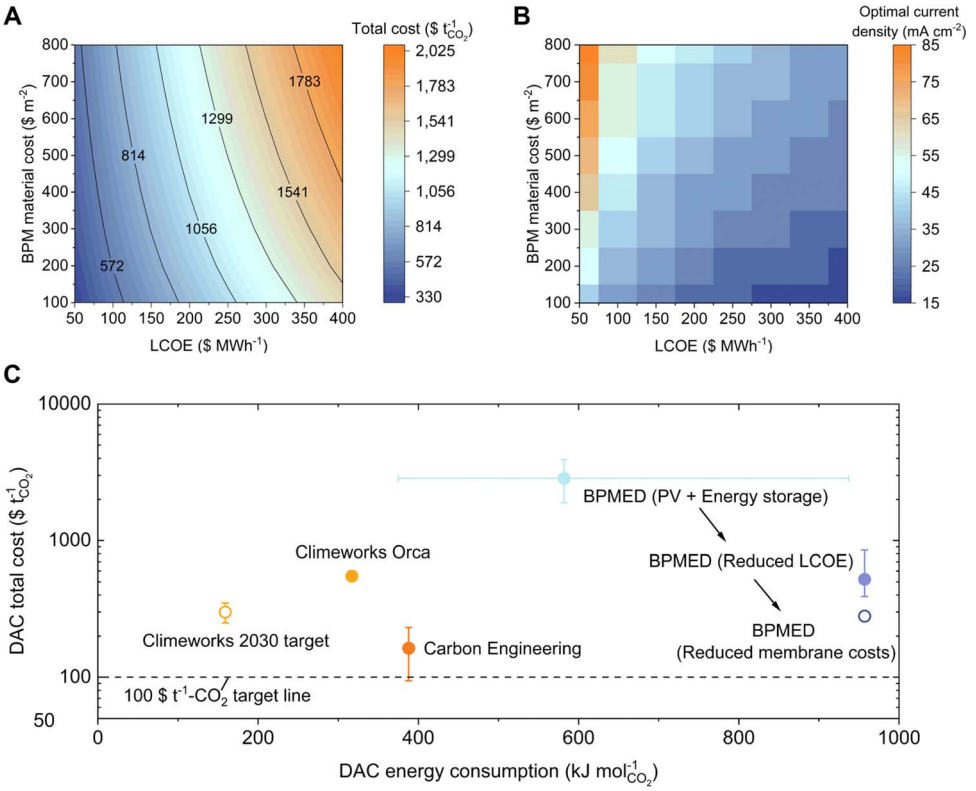

Fig. 7 Prospect of a solar-driven BPMEM DAC system. (A) Combined effect of future LCOE and material costs. (B) The optimal BPMED current density variation affected by the relative value of electricity and materials. (C) Comparison of total DAC cost and specific energy consumption for the BPMED DAC *versus* currently deployed DAC technologies.

once the supplied renewable electricity cost decreases to around 50 \$ MWh^{-1}, the BPMED systems are projected to reach a comparable total cost of roughly 500 \$ per t-CO_2 (Fig. 7A and C), similar to that of Climeworks' existing plants.

Further cost reductions will depend primarily on materials optimization. Climeworks has claimed that their next-generation structured sorbents may halve energy consumption and reduce DAC cost to 250–350 \$ per t-CO_2. By comparison, the BPMED approach relies heavily on reducing the cost of electrochemical components, particularly BPMs. As illustrated in Fig. 7A and C, achieving a BPM cost of around 100 \$ m^{-2} would enable BPMED DAC systems to fall onto the same near-future cost trajectory of 300 \$ per t-CO_2 as advanced thermally driven technologies. It should also be noted that, under reduced electricity cost scenarios, the predicted energy consumption of BPMED remains above 900 kJ per mol-CO_2, as higher current densities are favored to offset membrane-area-related costs. This further highlights the need for continued electrochemical advancements to lower the intrinsic energy demand at higher current densities and unlock the full potential of BPMED DAC.

Generalizable constraints and design principles for electrochemical DAC

The findings motivate a broader discussion of their implications for electrochemical DAC technologies beyond BPMED. Fig. 8A presents representative electrochemical architectures for CO_2 capture applications (details are provided in SI 12). The simulated BPMED operating voltage (for a single BPM unit) ranges from 1.0 to 2.4 V at current densities between 10 and 100 mA cm^{-1}. By contrast, lower operating voltages are widely reported for other electrochemical cells such as proton-coupled electrolysis, capacitive deionization, and redox-active carrier systems. The corresponding specific energy consumption for these alternatives is often reported below 300 kJ per mol-CO_2, indicating significant potential for further energy reduction through electrochemical engineering. Such improvements could lessen the heavy dependence on electricity supply and potentially reduce the total cost of electrochemical DAC.

However, two major uncertainties currently constrain their practical deployment. First, most electrochemical innovations remain in the early stages of development. The reported low cell voltages and energy consumptions are typically obtained under controlled laboratory conditions, and some systems have only been demonstrated for CO_2-rich sources (*e.g.*, flue gas) rather than atmospheric DAC. Consequently, the actual energy demand is likely to be higher in practical DAC applications. Second, these alternative electrochemical architectures similarly depend on specialized and costly materials, such as membranes (as illustrated in Fig. 8A), catalysts, or redox electrolytes. Although many demonstrate excellent electrochemical performance at small scale, their long-term stability and economics remain largely unproven. Comprehensive techno-

A

Electrochemical cell	BPMED	Proton-coupled electrolysis	Capacitive deionization	Redox-active carriers
Configuration	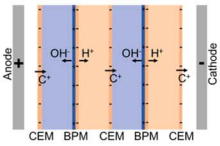	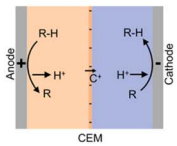	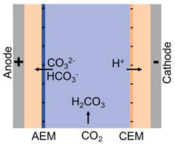	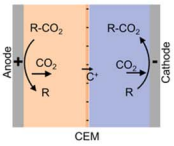
Membrane	BPM+CEM/AEM	CEM/AEM	CEM+AEM	CEM/AEM
Voltage range (V)	1.0-2.4	0.5-2.0	<1	0.2-1.2
Energy consumption (kJ mol^{-1}-CO_2)	375-937	100-300	30-60	≈100

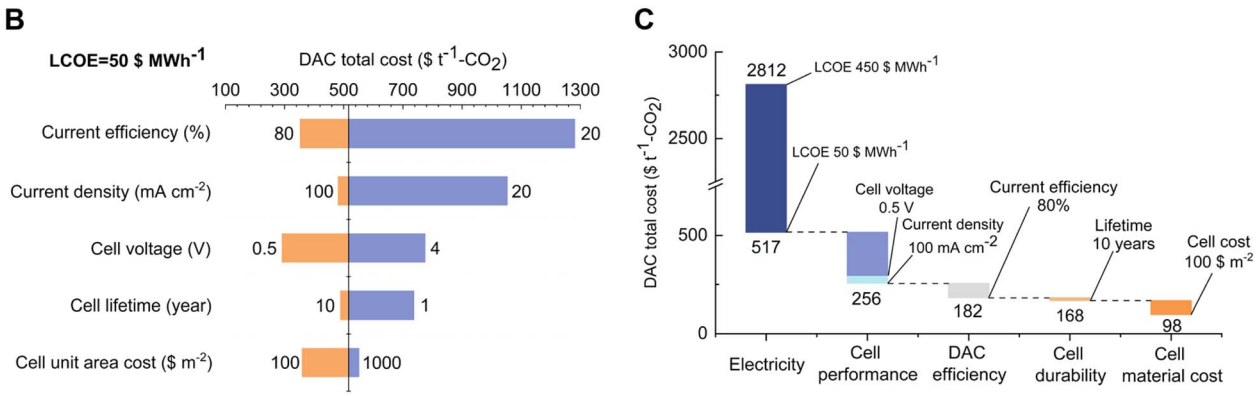

Fig. 8 Extended assessment of electrochemical DAC technologies and generalizable cost-reduction pathways. (A) Representative electrochemical CO_2-capture routes and their key operational and material characteristics (in the cell schematics, the cation (C^+) and CEM can be replaced by the corresponding anion and anion-exchange membrane, respectively). (B) Sensitivity of electrochemical DAC economics to key electrochemical performance parameters for the Shenzhen case, assuming an electricity cost of 50 \$ MWh^{-1}. (C) Illustrative cost-reduction pathway toward electrochemical DAC costs below 100 \$ per t-CO_2.

economic assessments are therefore essential to guide the design of more complex electrochemical reactors and operational strategies.

To capture the influence of performance variations across different electrochemical DAC devices, a set of key operating parameters is identified and controlled in the annual simulations. Details of the selected parameters are provided in SI 13. A sensitivity analysis is then performed to assess how uncertainties in electrochemical device performance affect the resulting system-level outcomes under constant renewable electricity supply conditions. All simulations are based on the Shenzhen case, with the LCOE fixed at 50 \$ MWh^{-1} throughout.

Fig. 8B illustrates the variation in the estimated DAC total cost resulting from changes in individual electrochemical system parameters. The baseline corresponds to the modeled BPMED system operating at a constant current density of 80 mA cm^{-2}, which represents the optimal current density under an electricity cost of 50 \$ MWh^{-1} (Fig. 7B). Under this baseline condition, the estimated DAC cost is approximately 500 \$ per t-CO_2. Relative to this baseline, the influence of current (faradaic) efficiency is the most pronounced. Here, current efficiency is defined as the fraction of the cell current that is directly converted to captured CO_2 (SI 13). As the current efficiency varies from 20% to 80%, the estimated DAC cost changes by more than a factor of three, ranging from 1280 to 353 \$ per t-CO_2. This strong sensitivity highlights the critical importance of charge utilization for CO_2 absorption and regeneration, under the inherently dilute conditions of atmospheric CO_2.

Cell-level electrochemical characteristics also have a notable influence on DAC cost, as reflected by the operating cell voltage and current density. These parameters directly determine the intrinsic power consumption and the required scale of the electrochemical device. For example, at an idealized low cell voltage of 0.5 V operated at 80 mA cm^{-2}, the estimated DAC cost is reduced to approximately 291 \$ per t-CO_2. In contrast, variations in the cell lifetime and unit-area cost over the investigated one-order-of-magnitude range show comparatively smaller effects on total DAC cost. Nevertheless, both parameters may span substantially wider ranges in practice, depending on the complexity of the electrochemical architecture, including the use of expensive or sensitive materials and the demands of complex operation.

Overall, the individual effects of the investigated electrochemical parameters on DAC cost are comparable in magnitude

and do not, by themselves, shift the system far from the baseline cost level. Moreover, compared with the modeled BPMED system, most existing electrochemical DAC technologies are reported or expected to exhibit similar overall energy consumption under practical operating conditions. As a result, the sensitivity analysis and cost trends derived from BPMED are broadly representative and can be extended to a wide range of electrochemical DAC systems.

Fig. 8C integrates the sensitivity insights from Fig. 8B into an illustrative cost-reduction pathway toward electrochemical DAC costs below 100 $ per t-CO_2. Consistent with the preceding analyses, the largest initial reduction in DAC cost arises from lowering the effective electricity cost, reflecting the dominant role of power generation and long-duration energy storage in renewable-driven DAC systems. Transitioning from a practical electricity cost of 450 $ MWh^{-1} to a favorable supply scenario of 50 450 $ MWh^{-1} yields a substantial decrease in total DAC cost, from over 2500 $ per t-CO_2 to 517 $ per t-CO_2.

Subsequent reductions are achieved through improvements in electrochemical cell and system performance, including increased current efficiency (80%), reduced operating voltage (0.5 V), and elevated current densities (>100 mA cm^{-2}). Together, these advances reduce the total DAC cost to below 200 $ per t-CO_2. Additional cost reductions arise from enhanced cell durability and reduced material costs, which lower replacement frequency and capital expenditure over the system lifetime. Under the combined effects of low-cost electricity supply, improved electrochemical performance, and enhanced materials durability and economy, a lower bound DAC cost of 98 $ per t-CO_2 is achieved. Although such idealized conditions may be challenging to realize in the near term, this analysis outlines a coherent and quantitative pathway toward the widely cited target of DAC costs below 100 $ per t-CO_2.

Conclusion

Electrochemical DAC offers a fully electrified and potentially scalable pathway for atmospheric carbon removal. In this work, we present a comprehensive techno-economic assessment of continuous BPMED-based DAC systems powered by intermittent solar electricity, explicitly accounting for diurnal and seasonal variability, energy storage requirements, and operational flexibility. By evaluating three representative system configurations—BPMED-PEMFC, BPMED-EL-PEMFC, and BPMED-BS systems—we demonstrate that the renewable electricity supply fundamentally governs system cost and feasibility.

Although battery-based storage achieves the highest energy efficiency (430 kJ per mol-CO_2), its reliance on large-scale, long-duration storage leads to prohibitively high system costs under strict off-grid operation. In contrast, hydrogen-based configurations reduce storage cost intensity, with the BPMED-PEMFC system achieving the lowest DAC cost of 2849 $ per t-CO_2 by exploiting inherent load-following behavior. Enabling active flexible BPMED operation (current density varying 10–90 mA cm^{-2}) further reduces DAC cost to 2163 $ per t-CO_2 by alleviating seasonal storage requirements.

Extending the analysis beyond off-grid operation, we show that electricity supply flexibility through limited grid assistance defines a practical lower bound for system-level electricity cost. When combined with operational flexibility and siting optimization, all three systems achieve LCOEs below 100 $ MWh^{-1} and DAC costs below 1000 $ per t-CO_2, establishing a realistic cost floor under renewable-dominated electricity supply. Under favorable future conditions, characterized by electricity costs of 50 $ MWh^{-1} and reduced membrane prices of 100 $ m^{-2}, BPMED-based DAC costs are projected to decrease to approximately 330 $ per t-CO_2.

Beyond BPMED-specific findings, this study demonstrates that the identified constraints and design principles arise from fundamental system-level interactions between electricity supply, electrochemical operation, and energy storage, and are therefore broadly applicable to electrochemical DAC technologies. Sensitivity and pathway analyses further indicate that achieving DAC costs near the widely cited target of 100 $ t^{-1} CO_2 will require coordinated progress across electricity supply, electrochemical performance, materials durability and economy.

Overall, this work provides a quantitative framework for evaluating electrochemical DAC under realistic renewable energy conditions and highlights the central role of system-level design in translating promising electrochemical performance into scalable and economically viable carbon removal. These insights inform both technology development and deployment strategies for next-generation electrochemical DAC systems integrated with low-carbon energy infrastructures.

Author contributions

Guokun Liu: conceptualization, methodology, formal analysis, investigation, data curation, writing – original draft. Yukun Zhang: methodology, investigation, data curation, writing – original draft. Meng Lin: conceptualization, validation, writing – review & editing, supervision. Aidong Yang: writing – review & editing, supervision.

Conflicts of interest

The authors declare no conflicts of interest.

Data availability

All data supporting the findings of this study are available within the article and its supplementary information (SI). Additional simulation data or model code used in this work are available from the corresponding author upon request. Supplementary information is available. See DOI: https://doi.org/10.1039/d6el00018e.

Acknowledgements

The Guangdong Major Project of Basic Research under Grant No. 2023B0303000002, SUSTech High Level of Special Funds under Grant No. G03034K001, National Natural Science

Foundations of China under Grant No. 52376191, and SUSTech Fellowship Program are acknowledged. Guokun Liu also acknowledges the support of the Clarendon Fund Scholarship and Nicholas Bratt Scholarship from the University of Oxford.

References

1 K. Ricke, L. Drouet, K. Caldeira and M. Tavoni, Country-level social cost of carbon, *Nat. Clim. Change*, 2018, **8**(10), 895–900.
2 J. Morris, A. Gurgel, B. K. Mignone, H. Kheshgi and S. Paltsev, Mutual reinforcement of land-based carbon dioxide removal and international emissions trading in deep decarbonization scenarios, *Nat. Commun.*, 2024, **15**(1), 7160.
3 Z. Liu, Z. Deng, S. Davis and P. Ciais, Monitoring global carbon emissions in 2022, *Nat. Rev. Earth Environ.*, 2023, **4**(4), 205–206.
4 R. Hanna, A. Abdulla, Y. Xu and D. G. Victor, Emergency deployment of direct air capture as a response to the climate crisis, *Nat. Commun.*, 2021, **12**(1), 368.
5 K. M. Diederichsen, R. Sharifian, J. S. Kang, Y. Liu, S. Kim, B. M. Gallant, *et al.*, Electrochemical methods for carbon dioxide separations, *Nat. Rev. Methods Primers*, 2022, **2**(1), 1–20.
6 R. M. Sharifian, R. Wagterveld, A. Digdaya I, C. A. Xiang and D. Vermaas, Electrochemical carbon dioxide capture to close the carbon cycle, *Energy Environ. Sci.*, 2021, **14**(2), 781–814.
7 S. Deutz and A. Bardow, Life-cycle assessment of an industrial direct air capture process based on temperature-vacuum swing adsorption, *Nat. Energy*, 2021, **6**(2), 203–213.
8 F. Sabatino, A. Grimm, F. Gallucci, M. van S. Annaland, G. J. Kramer and M. Gazzani, A comparative energy and costs assessment and optimization for direct air capture technologies, *Joule*, 2021, **5**(8), 2047–2076.
9 X. Zhu, W. Xie, J. Wu, Y. Miao, C. Xiang, C. Chen, *et al.*, Recent advances in direct air capture by adsorption, *Chem. Soc. Rev.*, 2022, **51**(15), 6574–6651.
10 C. Y. Chuah, Y. L. Ho, A. M. H. Syed, K. G. K. Thivyalakshmi, E. T. Yang, K. Johari, *et al.*, Applicability of Adsorbents in Direct Air Capture (DAC): Recent Progress and Future Perspectives, *Ind. Eng. Chem. Res.*, 2025, **64**(8), 4117–4147.
11 C. Beuttler, L. Charles and J. Wurzbacher, The Role of Direct Air Capture in Mitigation of Anthropogenic Greenhouse Gas Emissions, *Front. Clim.*, 2019, **1**, 10.
12 J. A. Wurzbacher, C. Gebald, S. Brunner and A. Steinfeld, Heat and mass transfer of temperature-vacuum swing desorption for CO_2 capture from air, *Chem. Eng. J.*, 2016, **283**, 1329–1338.
13 M. Steutermann, E. Simon, A. Prifti, S. Didas and B. Atherton, *Scaleup and Site-specific Engineering Design for Global Thermostat Direct Air Capture Technology*, Black & Veatch Corporation, Overland Park, KS (United States), 2024.
14 J. Young, N. McQueen, C. Charalambous, S. Foteinis, O. Hawrot, M. Ojeda, *et al.*, The cost of direct air capture and storage can be reduced via strategic deployment but is unlikely to fall below stated cost targets, *One Earth*, 2023, **6**(7), 899–917.
15 F. Bisotti, K. A. Hoff, A. Mathisen and J. Hovland, Direct Air capture (DAC) deployment: A review of the industrial deployment, *Chem. Eng. Sci.*, 2024, **283**, 119416.
16 B. Ge, C. Chen, Y. Xu, S. Roberts, M. Zhang, Q. Shao, *et al.*, Enhancing adsorbent performance for direct air capture of CO_2 by in-situ amine-grafting of layered double hydroxides, *Chem. Eng. J.*, 2024, **500**, 156782.
17 Y. Gomez-Rueda, B. Verougstraete, C. Ranga, E. Perez-Botella, F. Reniers and J. F. M. Denayer, Rapid temperature swing adsorption using microwave regeneration for carbon capture, *Chem. Eng. J.*, 2022, **446**, 137345.
18 H. E. Holmes, S. Banerjee, A. Vallace, R. P. Lively, C. W. Jones and M. J. Realff, Tuning sorbent properties to reduce the cost of direct air capture, *Energy Environ. Sci.*, 2024, **17**(13), 4544–4559.
19 A. A. Al-Absi, A. M. Benneker and N. Mahinpey, Amine Sorbents for Sustainable Direct Air Capture: Long-Term Stability and Extended Aging Study, *Energy Fuels*, 2024, **38**(10), 8938–8950.
20 G. H. Li and J. Yao, Direct Air Capture (DAC) for Achieving Net-Zero CO_2 Emissions: Advances, Applications, and Challenges, *Eng.*, 2024, **5**(3), 1298–1336.
21 G. Holmes and D. W. Keith, An air–liquid contactor for large-scale capture of CO_2 from air, *Philos. Trans. R. Soc., A*, 2012, **370**, 4380–4403.
22 D. W. Keith, G. Holmes, D. S. Angelo and K. Heidel, A Process for Capturing CO_2 from the Atmosphere, *Joule*, 2018, **2**(8), 1573–1594.
23 E. Wang, R. Navik, Y. H. Miao, Q. Gao, D. Izikowitz, L. Chen, *et al.*, Reviewing direct air capture startups and emerging technologies, *Cell Rep. Phys. Sci.*, 2024, **5**(2), 101791.
24 D. Krekel, R. C. Samsun, R. Peters and D. Stolten, The separation of CO_2 from ambient air - A techno-economic assessment, *Appl. Energy*, 2018, **218**, 361–381.
25 K. J. An, K. Li, C. M. Yang, J. Brechtl and K. Nawaz, A comprehensive review on regeneration strategies for direct air capture, *J. CO_2 Util.*, 2023, **76**, 102587.
26 N. McQueen, K. V. Gomes, C. McCormick, K. Blumanthal, M. Pisciotta and J. Wilcox, A review of direct air capture (DAC): scaling up commercial technologies and innovating for the future, *Prog. Energy*, 2021, **3**(3), 032001.
27 S. Jin, M. Wu, G. Gordon R, J. Aziz M and G. Kwabi D, pH swing cycle for CO_2 capture electrochemically driven through proton-coupled electron transfer, *Energy Environ. Sci.*, 2020, **13**(10), 3706–3722.
28 X. Zhang, Z. Fang, P. Zhu, Y. Xia and H. Wang, Electrochemical regeneration of high-purity CO_2 from (bi) carbonates in a porous solid electrolyte reactor for efficient carbon capture, *Nat. Energy*, 2025, **10**(1), 55–65.
29 S. Stucki, A. Schuler and M. Constantinescu, Coupled CO_2 recovery from the atmosphere and water electrolysis: Feasibility of a new process for hydrogen storage, *Int. J. Hydrogen Energy*, 1995, **20**(8), 653–663.

30 P. Zhu, Z. Y. Wu, A. Elgazzar, C. Dong, T. U. Wi, F. Y. Chen, *et al.*, Continuous carbon capture in an electrochemical solid-electrolyte reactor, *Nature*, 2023, **618**(7967), 959–966.
31 G. Zeng, J. Ye and M. Yan, Application of electrodeionization process for bioproduct recovery and CO_2 capture and storage, *Curr. Org. Chem.*, 2016, **20**(26), 2790–2798.
32 L. Legrand, O. Schaetzle, R. C. F. de Kler and H. V. M. Hamelers, Solvent-Free CO_2 Capture Using Membrane Capacitive Deionization, *Environ. Sci. Technol.*, 2018, **52**(16), 9478–9485.
33 H. Xie, Y. Wu, T. Liu, F. Wang, B. Chen and B. Liang, Low-energy-consumption electrochemical CO_2 capture driven by biomimetic phenazine derivatives redox medium, *Appl. Energy*, 2020, **259**, 114119.
34 S. Jin, M. Wu, Y. Jing, R. G. Gordon and M. J. Aziz, Low energy carbon capture via electrochemically induced pH swing with electrochemical rebalancing, *Nat. Commun.*, 2022, **13**(1), 2140.
35 T. N. D. Cao, S. W. Snyder, Y. I. Lin, Y. J. Lin, S. Negi and S. Y. Pan, Unraveling the Potential of Electrochemical pH-Swing Processes for Carbon Dioxide Capture and Utilization, *Ind. Eng. Chem. Res.*, 2023, **62**(49), 20979–20995.
36 M. D. Eisaman, L. Alvarado, D. Larner, P. Wang, B. Garg and K. A. Littau, CO_2 separation using bipolar membrane electrodialysis, *Energy Environ. Sci.*, 2011, **4**(4), 1319–1328.
37 M. D. Eisaman, L. Alvarado, D. Larner, P. Wang and K. A. Littau, CO_2 desorption using high-pressure bipolar membrane electrodialysis, *Energy Environ. Sci.*, 2011, **4**(10), 4031–4037.
38 M. D. Eisaman, K. Parajuly, A. Tuganov, C. Eldershaw, N. Chang and K. A. Littau, CO_2 extraction from seawater using bipolar membrane electrodialysis, *Energy Environ. Sci.*, 2012, **5**(6), 7346–7352.
39 A. Iizuka, K. Hashimoto, H. Nagasawa, K. Kumagai, Y. Yanagisawa and A. Yamasaki, Carbon dioxide recovery from carbonate solutions using bipolar membrane electrodialysis, *Sep. Purif. Technol.*, 2012, **101**, 49–59.
40 S. Valluri and S. K. Kawatra, Reduced reagent regeneration energy for CO_2 capture with bipolar membrane electrodialysis, *Fuel Process. Technol.*, 2021, **213**, 106691.
41 S. Vallejo Castaño, Q. Shu, M. Shi, R. Blauw, P. Loldrup Fosbøl, P. Kuntke, *et al.*, Optimizing alkaline solvent regeneration through bipolar membrane electrodialysis for carbon capture, *Chem. Eng. J.*, 2024, **488**, 150870.
42 Y. Huang, D. Xu, S. Deng and M. Lin, A hybrid electro-thermochemical device for methane production from the air, *Nat. Commun.*, 2024, **15**(1), 8935.
43 F. Sabatino, M. Mehta, A. Grimm, M. Gazzani, F. Gallucci, G. J. Kramer, *et al.*, Evaluation of a Direct Air Capture Process Combining Wet Scrubbing and Bipolar Membrane Electrodialysis, *Ind. Eng. Chem. Res.*, 2020, **59**(15), 7007–7020.
44 F. Sabatino, M. Gazzani, F. Gallucci and M. V. Annaland, Modeling, Optimization, and Techno-Economic Analysis of Bipolar Membrane Electrodialysis for Direct Air Capture Processes, *Ind. Eng. Chem. Res.*, 2022, **61**(34), 12668–12679.
45 Y. Zhao, J. Wang, Z. Ji, J. Liu, X. Guo and J. Yuan, A novel technology of carbon dioxide adsorption and mineralization via seawater decalcification by bipolar membrane electrodialysis system with a crystallizer, *Chem. Eng. J.*, 2020, **381**, 122542.
46 R. Sharifian, L. Boer, R. M. Wagterveld and D. A. Vermaas, Oceanic carbon capture through electrochemically induced in situ carbonate mineralization using bipolar membrane, *Chem. Eng. J.*, 2022, **438**, 135326.
47 I. A. Digdaya, I. Sullivan, M. Lin, L. Han, W. H. Cheng, H. A. Atwater, *et al.*, A direct coupled electrochemical system for capture and conversion of CO_2 from oceanwater, *Nat. Commun.*, 2020, **11**(1), 4412.
48 M. Aliaskari, J. Wezstein, F. Saravia and H. Horn, A systematic analysis of operating parameters for CO_2 capture from seawater by Bipolar Membrane Electrodialysis (BPMED), *Sep. Purif. Technol.*, 2024, **339**, 126679.
49 R. Pärnamäe, L. Gurreri, J. Post, W. J. van Egmond, A. Culcasi, M. Saakes, *et al.*, The Acid–Base Flow Battery: Sustainable Energy Storage via Reversible Water Dissociation with Bipolar Membranes, *Membranes*, 2020, **10**(12), 409.
50 M. Gür T, Review of electrical energy storage technologies, materials and systems: challenges and prospects for large-scale grid storage, *Energy Environ. Sci.*, 2018, **11**(10), 2696–2767.
51 J. Guerra O, J. Zhang, J. Eichman, P. Denholm, J. Kurtz and B. M. Hodge, The value of seasonal energy storage technologies for the integration of wind and solar power, *Energy Environ. Sci.*, 2020, **13**(7), 1909–1922.
52 G. Realmonte, L. Drouet, A. Gambhir, J. Glynn, A. Hawkes, A. C. Köberle, *et al.*, An inter-model assessment of the role of direct air capture in deep mitigation pathways, *Nat. Commun.*, 2019, **10**(1), 3277.
53 S. Pang, S. Jin, F. Yang, M. Alberts, L. Li, D. Xi, *et al.*, A phenazine-based high-capacity and high-stability electrochemical CO_2 capture cell with coupled electricity storage, *Nat. Energy*, 2023, **8**(10), 1126–1136.
54 R. Silcox and R. Bala Chandran, Demand-side flexibility enables cost savings in a reversible pH-swing electrochemical process for oceanic CO_2 removal, *Cell Rep. Phys. Sci.*, 2024, **5**(3), 101884.
55 W. Jiang, W. Liu, Y. Wang, Z. Zhao, Q. Li, Y. Wu, *et al.*, Electrochemically Regenerated Amine for CO_2 Capture Driven by a Proton-Coupled Electron Transfer Reaction, *Ind. Eng. Chem. Res.*, 2022, **61**(36), 13578–13588.
56 G. Liu, A. Yang and R. C. Darton, Numerical Modeling and Comparative Analysis of Electrolysis and Electrodialysis Systems for Direct Air Capture, *ACS Sustain. Chem. Eng.*, 2024, **12**(10), 3951–3965.
57 A. A. Belsky, D. Y. Glukhanich, M. J. Carrizosa and V. V. Starshaia, Analysis of specifications of solar photovoltaic panels, *Renew. Sustain. Energy Rev.*, 2022, **159**, 112239.

58 B. Flamm, C. Peter, F. N. Büchi and J. Lygeros, Electrolyzer modeling and real-time control for optimized production of hydrogen gas, *Appl. Energy*, 2021, **281**, 116031.
59 Y. Wang, Y. Pang, H. Xu, A. Martinez and S. Chen K, PEM Fuel cell and electrolysis cell technologies and hydrogen infrastructure development – a review, *Energy Environ. Sci.*, 2022, **15**(6), 2288–2328.
60 A. V. Vykhodtsev, D. Jang, Q. Wang, W. Rosehart and H. Zareipour, A review of modelling approaches to characterize lithium-ion battery energy storage systems in techno-economic analyses of power systems, *Renew. Sustain. Energy Rev.*, 2022, **166**, 112584.
61 European Commission, Joint Research Centre. Photovoltaic Geographical Information System (PVGIS): Solar radiation, 2023.
62 J. M. Weinand, M. Hoffmann, J. Göpfert, T. Terlouw, J. Schönau, P. Kuckertz, *et al.*, Global LCOEs of decentralized off-grid renewable energy systems, *Renew. Sustain. Energy Rev.*, 2023, **183**, 113478.
63 X. Lu, S. Chen, C. P. Nielsen, C. Zhang, J. Li, H. Xu, *et al.*, Combined solar power and storage as cost-competitive and grid-compatible supply for China's future carbon-neutral electricity system, *Proc. Natl. Acad. Sci. U. S. A.*, 2021, **118**(42), e2103471118.
64 A. M. Adeyinka, O. C. Esan, A. O. Ijaola and P. K. Farayibi, Advancements in hybrid energy storage systems for enhancing renewable energy-to-grid integration, *Sustain. Energy Res.*, 2024, **11**(1), 26.
65 C. A. Hunter, M. M. Penev, E. P. Reznicek, J. Eichman, N. Rustagi and S. F. Baldwin, Techno-economic analysis of long-duration energy storage and flexible power generation technologies to support high-variable renewable energy grids, *Joule*, 2021, **5**(8), 2077–2101.